Size versus Slenderness: Two Competing Parameters in the Seismic Stability of Free-Standing Rocking Columns

Nicos Makris[1] and Georgios Kampas[2]

Abstract

When a free-standing column with a given base becomes taller and taller, there is a competition between the increase in its size (more stable) and the increase in its slenderness (less stable). This paper investigates how these two competing phenomena affect the stability of tall, slender, free-standing columns when subjected to horizontal and vertical ground shaking. The main conclusion of the paper is that the outcome of this competition is sensitive to local details of the ground shaking and the dominant frequency of a possible coherent, distinguishable pulse. The often observed increase in stability due to increase in height (despite the increase in slenderness) may be further enhanced due to a sudden transition from the lower mode of overturning with impact to the higher mode of overturning without impact. The paper proceeds by offering a simple mathematical explanation why the vertical ground acceleration has a marginal effect on the stability of a slender, free-standing column; and concludes that the level of ground shaking that is needed to overturn a tall free-standing column of any size and any slenderness is a decreasing function of the length scale, $a_p T_p^2$ of the dominant coherent acceleration pulse normalized to the base-width of the column.

Introduction

During ground shaking, the more slender among two equally tall structures is less stable and one can show via static equilibrium that the ground acceleration needed to uplift a free-standing rectangular column is g (width/height). Nevertheless; upon uplifting, there is a safety margin between uplifting and overturning of slender, free-standing columns and that as the size of the column increases (when the slenderness is kept constant) this safety margin increases appreciably to the extent that large free-standing columns enjoy ample seismic stability (Kirkpatric 1927, Housner 1963, Yim et al. 1980, Ishiyama 1982, Zhang and Makris 2001, Konstantinidis and Makris 2005, Makris 2014 and references report therein). Accordingly, when a column with a given base $= 2b$, becomes taller and taller, there is a competition between the increase in the size of the column (more stable) and the increase in its slenderness (less stable). This paper investigates how these two competing phenomena affect the stability of tall, slender, free-standing columns when subjected to horizontal and vertical ground shaking. The findings of this study are used to assess the trend through the centuries of increasing the size and slenderness of free-standing columns that create the emblematic peristyles of archaic, classical and roman temples. Our findings have also implications in the design of tall bridge piers where the concept of rocking isolation becomes attractive (Makris and Vassiliou 2014, Makris 2014).

Figure 1 shows the size and slenderness of selected monolithic columns from the peristyles of ancient temples ranging from the archaic period to the early roman period (Powell 1905, Dinsmoor 1975, Mark 1993, Fletcher 2001). Interestingly, with the exception of the slenderness of the column from the Temple of Olympic Zeus in Syracuse (480 B.C.), the general trend is that the slenderness of monolithic columns increases with time; while, some of the columns built in the

A.D. years assume very large size while being most slender ($\tan a \le 0.1$, Dinsmoor 1975, Fletcher 2001).

This paper presents a comprehensive stability analysis together with the associated overturning diagrams of three free-standing columns having width at their base, $2b = 1.0m$, $2.0m$ and $4.0m$ (as shown in Figure 2). The height of each column during the stability analysis with a given base is increased incrementally in order to create larger columns with larger slenderness values. Both horizontal and vertical ground accelerations are considered.

Equation of motion of a free-standing rocking column subjected to Horizontal and Vertical Accelerations

With reference to Figure 3 and assuming that the coefficient of friction is large enough so that there is no sliding, the equation of motion of a free-standing column with size $R = \sqrt{h^2 + b^2}$, slenderness $\alpha = \tan^{-1}(b/h)$ and rotational inertia I_0 subjected to a horizontal and a vertical ground acceleration, $\ddot{u}_g(t)$ and $\ddot{v}_g(t)$ respectively, when rocking around O and O', is (Yim et al.1980; Ishiyama 1982; Taniguchi 2002 and references report therein)

$$I_0\ddot{\theta}(t) + mgR\sin[-\alpha - \theta(t)] = -m\ddot{u}_g(t)R\cos[-\alpha - \theta(t)] - m\ddot{v}_g(t)R\sin[-\alpha - \theta(t)], \quad \theta(t) < 0 \quad (1)$$

$$I_0\ddot{\theta}(t) + mgR\sin[\alpha - \theta(t)] = -m\ddot{u}_g(t)R\cos[\alpha - \theta(t)] - m\ddot{v}_g(t)R\sin[\alpha - \theta(t)], \quad \theta(t) > 0 \quad (2)$$

Rocking motion initiates when, $\ddot{u}_g(t) > (1 + \frac{\ddot{v}_g(t)}{g})g\tan\alpha$. The aforementioned equations of motion can be expressed in the compact form (Zhang and Makris 2001, Makris and Vassiliou 2012)

$$\ddot{\theta}(t) = -p^2\{(1+\frac{\ddot{v}_g(t)}{g})\sin[\alpha\,\mathrm{sgn}(\theta(t))-\theta(t)] + \frac{\ddot{u}_g(t)}{g}\cos[\alpha\,\mathrm{sgn}(\theta(t))-\theta(t)]\} \tag{3}$$

In equation (3), the quantity $p=\sqrt{mRg/I_o}$ is the frequency parameter of the block and is an expression of its size. For rectangular blocks, $p=\sqrt{3g/(4R)}$. Accordingly, overturning diagrams where the horizontal axis is the size of the column, R, can also be viewed as overturning spectra given the one-to-one correspondence between the frequency parameter, p, and the size, R of the column.

The oscillation frequency of a rocking column under free vibration is not constant because it strongly depends on the vibration amplitude (Housner 1963, Yim et al.1980). Nevertheless, the quantity $p=\sqrt{3g/(4R)}$ is a measure of the dynamic characteristics of the column given that it is the natural frequency of a rectangular plane with diagonal $=2R$ that is hanging by one of its top corners. For the $7.24m \times 1.74m$ free-standing column of the Temple of Apollo in Corinth (Dinsmoor 1975), $p=1.4rad/s$, whereas for the tall piers of a valley bridge ($2h>20m$), $p \approx 0.8rad/s$ or even less.

Figure 3(right) shows the moment-rotation relationship during the rocking motion of a free-standing column. The system has infinite stiffness until the magnitude of the applied moment reaches the value $mgR\sin\alpha$ (without vertical acceleration), and once the column is rocking, its restoring force decreases monotonically, reaching zero when $\theta=\alpha$.

During rocking motion the ratio of kinetic energy before and after the impact is $r=\dot{\theta}_2^{\,2}/\dot{\theta}_1^{\,2}$; which means that the angular velocity after the impact is only $\sqrt{r}$ times the velocity before the impact. Conservation of angular momentum just before and right after the impact gives (Housner 1963):

$$r = \left[1 - \frac{3}{2}\sin^2 \alpha\right]^2 \tag{4}$$

The value of the coefficient of restitution given by equation (4) is the maximum value needed for a free-standing rigid block with slenderness α to undergo rocking motion. Larger values of the coefficient of restitution than the upper bound value given by equation (4) result to loss of contact (jumps) during impact. In the event that additional energy is lost because of the inelastic behavior during impact, the value of the actual coefficient of restitution r will be less than the one computed from equation (4).

Overturning Spectra due to Idealized Pulse-Excitations and the Implications of Multiple Modes of Overturning

Over the last half century an ever increasing database of recorded ground motions has shown that the kinematic characteristics of the ground near the fault of earthquakes contain distinguishable acceleration pulses. The early work of Veletsos et al. (1965) on producing elastic and inelastic spectra due to pulse excitations was followed by the papers of Bolt (1976), Singh (1985), Somerville and Graves (1993), Hall et al. (1995), Makris (1997), Somerville (1998), Makris and Chang (2000a,b), Abrahamson (2001), Alavi and Krawinkler (2001), and more recently by the papers of Mavroeidis and Papageorgiou (2003), Baker (2007) and Vassiliou and Makris (2011) who used the Mavroeidis and Papageorgiou model (2003) in association with wavelet analysis to develop a mathematically formal and objective procedure to extract the time scale, T_p, and length scale, $a_p T_p^{\,2}$, of strong ground motions.

The identification of the pulse period, T_p, and the pulse amplitude, a_p, of the dominant coherent pulse is of particular interest because the product, $a_p T_p{}^2 = L_e$, is a characteristic length scale of the ground excitation and is a measure of the persistence of the most energetic pulse to generate inelastic deformation (Makris and Black 2004a,b). The persistence of the pulse, $a_p T_p{}^2 = L_e$, is a different characteristic than the strength of the pulse that is measured with the peak pulse acceleration, a_p (Makris and Black 2004a,b, Makris and Psychogios, 2006 Karavasilis et al.2010). This paper shows that the level of the overturning acceleration from several pulse-like records exhibit a decreasing trend when ordered with the characteristic length scale, $L_e = a_p T_p{}^2$, of the coherent pulse of the records used. The solid dark line in Figure 4(a) that approximates the long-period acceleration pulse of the NS component of the Takarazuka motion recorded during the January 17, 1995 Kobe earthquake is a scaled expression of the symmetric Ricker wavelet (Ricker 1943; 1944)

$$\psi(t) = a_p \left(1 - \frac{2\pi^2 t^2}{T_p{}^2} \right) e^{-\frac{1}{2}\frac{2\pi^2 t^2}{T_p{}^2}} \tag{5}$$

The value of $T_p = 2\pi / \omega_p$ is the period that maximizes the Fourier spectrum of the symmetric Ricker wavelet. Similarly, the solid line in Figure 4(b), which approximates the long-period acceleration pulse of the Gilroy, Array #6, fault normal motion recorded during the 1979 Coyote Lake, California earthquake, is a scaled expression of the antisymmetric Ricker wavelet (Ricker 1943, 1944, Vassiliou and Makris 2011).

$$\psi(t) = \frac{a_p}{\beta} \left(\frac{4\pi^2 t^2}{3T_p{}^2} - 3 \right) t e^{-\frac{1}{2}\frac{4\pi^2 t^2}{3T_p{}^2}} \tag{6}$$

in which β is a factor equal to 1.3801 that enforces the aforementioned function to have a maximum equal to a_p.

Prior to the work on wavelike functions and wavelet analysis (Mavroeidis and Papageorgiou 2003, Baker 2007, Makris and Vassiliou 2011) simple trigonometric pulses have been proposed by the senior author and his coworkers (Makris 1997; Makris and Chang 2000a,b; Makris and Black 2004a,b) to extract the period and amplitude of the coherent distinguishable pulse. For instance, the heavy line in Figure 4(c) which approximates the strong coherent acceleration pulse of the OTE record from the 1973 Lefkada, Greece earthquake is a one-sine acceleration pulse

$$\ddot{u}_g(t) = a_p \sin(\omega_n t), \quad 0 < t < T_p \tag{7}$$

The various mathematical idealizations of coherent pulse-type ground motions as described by equations (7)-(9) and shown in Figure 4 are invariably characterized by a pulse period, $T_p = \dfrac{2\pi}{\omega_p}$, and a pulse acceleration amplitude, a_p. From equation (3), the response of a free-standing rocking column subjected to a horizontal ground acceleration pulse only, is a function of five variables

$$\theta(t) = f(p, \alpha, g, a_p, \omega_p) \tag{8}$$

According to the Vashy-Buckingham Π-theorem (Barenblatt 1996, Makris and Vassiliou 2012) equation (8) can be expressed in terms of dimensionless Π-products

$$\theta(t) = \varphi\left(\frac{\omega_p}{p}, \tan\alpha, \frac{a_p}{g}\right) \tag{9}$$

where $\Pi_\theta = \theta$, $\Pi_\omega = \dfrac{\omega_p}{p}$, $\Pi_a = \tan\alpha$ and $\Pi_g = \dfrac{a_p}{g}$.

Figure 5 shows the overturning acceleration spectrum of a rigid block with slenderness $a = 14^o$ ($b/h = \tan\alpha = 0.25$) due to one-sine acceleration pulse. Figure 5 indicates that as $\Pi_\omega = \frac{\omega_p}{p}$ increases, the acceleration needed to overturn the free-standing column becomes appreciably larger than the one needed to uplift it $= g\tan\alpha$. Most importantly, Figure 5 shows that in the case of a one-sine pulse there are two distinct modes of overturning: (I) overturning with one impact, and (II) overturning without impact. These two modes of overturning exist for columns up to a certain size (that is $\omega_p / p = 8.2$ when $\tan\alpha = 0.25$); whereas, larger columns excited to higher frequency pulses overturn only without impact (mode II).

This bifurcation phenomenon –that beyond a certain size a free-standing column overturns only without impact; therefore, a much larger acceleration is needed to create overturning –has important implications on the stability of freestanding columns. This is because, a tall and most slender column that is large enough so that it can only overturn without impact; may be more stable than a shorter (less slender) column with the same base that can overturn with one impact.

Overturning Diagrams due to Idealized Pulses-Horizontal Accelerations Only

In an effort to assess the competing effects of size and slenderness, Figure 6 plots the minimum overturning acceleration of a one-sine pulse that is needed to overturn a column with base $2b = 1m$ (left –say a column from the Temple of Aphaea, Aigina, Greece or a column from the Temple of Zeus, Aezanoi, Turkey –see Figure 1); a column with base $2b = 2m$ (center –say a column from the Temple of Apollo, Syracuse, Italy) and a column with base $2b = 4m$(right –say one of the center piers of a modern valley bridge). The horizontal axis shows the size of the column, R in meters, and all three plots originate at a value of R that corresponds to a minimum slenderness $\tan\alpha = 1/4$. In each plot, results are plotted for different values of the duration, T_p, of the pulse ($T_p = 0.50s$, $0.75s$, $1.00s$ and $1.50s$ -see Figure 4). Since each plot is for a given value of the column base, in each plot the slenderness of the column increases as the size R increases.

Figure 6 shows a remarkable result –that for moderately-long duration pulses (say as long as $T_p = 1.0s$) the increase in the column size offsets the anticipated decrease in the column stability due to the increase in slenderness. Interestingly, for values of $\tan\alpha \geq 1/8$ a further increase in the column height (further increase in the slenderness), the overturning diagrams assume a slightly positive slope indicating that size "wins" over slenderness. On the other hand, for the longer duration pulse where $T_p = 1.50s$, the overturning diagrams assume a negative slope indicating that slenderness prevails over size.

The two opposite trends can be explained by examining the participation on the moment of inertia of the column (proportional to the square of the size) in the equation of motion given by (3). In the event of a long duration pulse (a slowly increasing ground acceleration), upon the column uplifts ($\ddot{u}_g(t) > g\tan\alpha$) it will rotate slowly developing a feeble angular acceleration. Given the low angular acceleration the engagement of the rotational inertia (proportional to R^2) of the column is weak and in this case the slenderness of the column has a dominant effect over size.

In the event of a shorter duration pulse (more high-frequency pulse), the free-standing column experiences finite rotational accelerations which engage vividly the rotational inertia of the column (Makris 2014). In this case the dynamic seismic resistance of the free-standing column is enhanced with the active participation of its rotational inertia –a quantity that is proportional to the square of the column size. Accordingly, in this case the increase in the size of the column offsets the effect due to the increase of the slenderness.

Figure 7 plots the minimum overturning acceleration of a symmetric Ricker wavelet that is needed to overturn the three free-standing columns shown in Figure 2 with base $2b = 1.0m, 2.0m$ and $4.0m$. Again the horizontal axis expresses the size of the column, R, in meters and all three plots originate at a value of R that corresponds to a minimum slenderness of $s = 1/4$. In each plot, results are plotted for different values of the duration, T_p of the Ricker pulse. For the column with width $2b = 4.0m$, the overturning acceleration amplitudes that correspond to a duration of $T_p = 0.5s$ are not shown because they are exceedingly large (over 20g). In each plot as the size R increases, the slenderness of the column also increases given that each plot is for a given value of a column base.

Bifurcation to a higher overturning mode

In Figure 7, in addition to the trends that were observed and discussed in Figure 6 (overturning diagrams for a one-sine pulse) we observe a new trend that is due to the multiple modes of overturning discussed in the previous section. In all three plots shown in Figure 7, there are occasions where the overturning diagrams show a sudden jump to higher overturning accelerations. This happens because as the size of the column increases (even if it becomes more slender) the column assumes a size that is large enough so it can no longer overturn with one impact; and it can only overturn without impact –therefore, requiring an appreciable larger overturning acceleration. It is because of this bifurcation phenomenon (transitioning to a higher overturning mode) that a tall and slender column may be appreciably more stable than a much shorter column with the same base $= 2b$. For instance, Figure 7 (center, $2b = 2.0m$) indicates that when a column with slenderness $= 1/8$ ($16m$ tall) is excited by a Ricker pulse with period

$= T_p = 0.75s$ it is more stable that the column with the same base ($2b = 2.0m$) and slenderness, $s = 1/6$ ($12.0m$ tall).

Figure 8 illustrates this bahavior by plotting rotation and angular velocity time histories of two columns having width $2b = 2.0m$ and heights $2h = 12.0m$ (left) and $2h = 16.0m$ (right). The $12.0m$ tall column on the left overturns with one impact (the rotation history crosses the $\theta(t)/\alpha = 0$ line). On the other hand the $16.0m$ tall column on the right experiences an initial very high rotation without overturning and during the course of re-centering it reverses its motion prior to impact and overturns without experiencing any impact.

Figure 9 illustrates the same behavior by plotting the rotation and angular velocity time history of the two columns having width $2b = 4.0m$ and heights $2h = 20.0m$ (left) and $2h = 24.0m$ (right). Clearly, the behavior illustrated in Figures 8 and 9 is mainly due to the smooth shape of the single-frequency Ricker wavelet input. In the event of a recorded earthquake ground motion that contains several frequencies this kind of behavior is harder to observe; nevertheless, it may happen. For instance, in his seminal paper Ishiyama (1982) characterizes the seismic response and overturning of free-standing column as "*highly irregular given that taller columns are sometimes more stable than shorter ones of the same breadth*". The analysis presented in this section offers a physically motivated explanation for the reason that in some occasions size prevails over slenderness.

Nearly Self-Similar Response

The overturning diagrams shown in Figure 6 and 7 have significant practical value since they reveal in a direct way the remarkable result, that for moderately long duration pulses the increase in the column size not only can offset the anticipated decrease in the column stability due to the increase of slenderness, but in some occasions it may increase appreciably its stability.

We are now interested to examine whether the several response diagrams appearing in Figures 6 (of Figure 7) are related to each other; or whether each one contains independent information. Equation (9) dictates that in order to uncover any manifestation of self-similar behavior, the overturning acceleration values need to be expressed in terms of the dimensionless products, $\Pi_\omega = \omega_p / p$, $\Pi_a = \tan\alpha$ and $\Pi_g = a_p / g$.

Figure 10 indicates that when the overturning acceleration values are plotted in terms of the dimensionless products (Π_g / Π_a vs , Π_ω) all data presented on the three subplots of Figure 7 or Figure 8 are crowded together; without however collapsing precisely to a single master curve for overturning with one impact and a different master curve for overturning without impact. This is because the plots shown in Figure 10 are for all slenderness values (any $\tan\alpha \le 1/4$). In reality, the dynamics of the free-standing rocking column is governed by three dimensionless products ($\Pi_\omega = \dfrac{\omega_p}{p}, \Pi_g = \dfrac{a_p}{g}, \Pi_\alpha = \tan\alpha$) and only when the overturning spectra are plotted for a single slenderness (as is the overturning spectrum shown in Figure 5), the data are mathematically self-similar.

Response to Earthquake Excitation-Effect of the Vertical Component

Our investigation proceeds by examining how size and slenderness affect the stability of tall, slender, free-standing columns when excited by recorded ground motions. Our numerical investigation first focuses on the monolithic columns of: (a) the Temple of Aphaia, Aegina, Greece ($2b = 0.99m$, $2h = 5.27m$, $\tan\alpha = 0.101$); and (b) the Temple of Zeus, Aezanoi, Turkey (

$2b = 0.97m$, $2h = 9.55m$, $\tan \alpha = 0.101$). Given that the base-width of these two columns is almost one meter, the results from the earthquake response analysis can be compared with the results from the overturning spectra for $2b = 1.0m$ under pulse excitations presented at the left of Figures 6 and 7.

Figure 11 plots the rotation and angular velocity time histories at the verge of overturning of the two abovementioned free-standing columns when excited by the amplified horizontal only (left) and horizontal and vertical components (right) of the OTE ground motion recorded during the 1973 Lefkada, Greece earthquake. In this work, overturning of the free-standing columns is achieved by gradually amplifying the horizontal and vertical recorded motions by the same multiplication factor as if the columns were tested physically on a shaking table.

The first observation, is that the vertical acceleration has a marginal effect on the dynamics of rocking and it confirms the same observation made by Ishiyama (1982) more than three decades ago. For instance, the Aphaia-Aegina column overturns at 1.784 times the horizontal component of the 1973 Lefkada record ($PGA = 0.95g$); whereas it overturns at 1.766 times the horizontal and vertical component of the same record ($PGA = 0.94g$). Interestingly, the Zeus-Aezanoi column survives a higher level of horizontal ($PGA = 0.86g$) and vertical acceleration ($PGA = 0.13g$) than when excited by a horizontal acceleration ($PGA = 0.84g$) alone.

There are three reasons for the marginal importance to overturning of the vertical component of the ground motion. The first and foremost reason is the structure of the equation of motion given by equation (3). In equation (3) the horizontal input acceleration, $\ddot{u}_g(t)$, is multiplied with $\cos[\alpha - \theta(t)]$; whereas, the vertical input acceleration is multiplied with $\sin[\alpha - \theta(t)]$. Given that we are dealing with slender columns ($\tan \alpha < 0.25$), the quantity, $\cos[\alpha - \theta(t)]$, is of the order of one; whereas, $\sin[\alpha - \theta(t)]$ is of the order of $\alpha - \theta(t)$; which is a small angle. Accordingly, even if there is a strong vertical ground acceleration, it enters the dynamics of rocking after being suppressed with the factor $\alpha - \theta(t) << 1$. The second reason for the marginal importance of the vertical component of the ground motion is that in general it is a much more high-frequency ground motion; therefore, it has limited influence on the dynamics of a larger column with appreciable rotational inertia. The third reason is that the level of the vertical acceleration is in general lower than the level of the horizontal component. The marginal effect of the vertical acceleration on the rocking response of the free-standing columns is also shown in the subsequent response analysis histories presented in this paper.

Our numerical investigation proceeds with the dynamic response analysis of (a) the monolithic column from the Temple of Apollo, Syracuse, Italy ($2b = 2.0m$, $2h = 7.98m$, $\tan\alpha = 0.252$); and (b) a taller column with the same base, $2b = 2.0m$ and a height, $2h = 16.0m$ ($\tan\alpha = 0.125$).

Figure 12 plots rotation and angular velocity time histories at the verge of overturning of the two abovementioned free-standing columns when excited by the amplified horizontal (GIC-180) only (left) and the horizontal (GIC-180) and vertical components (right) of the Geotechnical Investigation Center ground motions recorded during the 1986 San Salvador earthquake. The interesting observation in this case is that when only the horizontal acceleration is considered (GIC-180) the Apollo Syracuse column overturns at 7.89 times the horizontal component of the GIC-180 record ($PGA = 3.75g$); whereas, the two times taller and two times more slender column shown at the bottom of Figure 13 needs 8.95 times the same acceleration record to overturn ($PGA = 4.25g$); confirming to a certain extent the findings uncovered with the overturning diagrams shown in Figure 7. The same trend is observed when the two columns of interest are subjected to the horizontal (GIC-180) and vertical components of the Geotechnical Investigation Center showing that a higher acceleration level is needed to topple the taller and more slender column.

Clearly, while this behavior shown in Figure 12 documents the appreciable contribution of the size to the column's stability, it needs to be recognized that such behavior is sensitive to the local kinematic characteristics of the ground motion. Figure 13 plots rotation and angular velocity time histories at the verge of overturning of the same two columns appearing in Figure 12 when excited by the amplified horizontal (GIC-90) only (left) and the horizontal (GIC-90) and vertical component (right) of the Geotechnical Investigation Center ground motions recorded during the 1986 San Salvador earthquake. In this case, when only the horizontal acceleration is considered (GIC-90), the Apollo Syracuse column survives a higher acceleration level ($PGA = 4.94g$) than the two-times taller and two-times more slender column which overturns with a $PGA = 4.14g$ acceleration level. Interestingly, the situation is again reversed when in addition to the horizontal acceleration (GIC-90), the vertical acceleration is also considered.

Figure 14 plots the best matching acceleration wavelet on the GIC-180(a) and GIC-90(b) components of the GIC ground motion recorded during the 1986 San Salvador earthquake. While macroscopically both records are best fitted by essentially the same wavelet (there is only a small difference of a 1/10 of a second in the duration, T_p, of the predominant pulse); the results presented in Figures 12 and 13 show that it is the local kinematic characteristics of the ground motion that control the final outcome–that is whether eventually size prevails on slenderness (see Figures 13 and 14).

The parameters a_p, T_p, φ and γ of the best matching wavelets of the GIC-180 and GIC-90 records shown in Figure 14 have been obtained by employing the extended wavelet transform proposed by Vassiliou and Makris (2011) where in addition to a time translation and a dilation-contraction, the proposed transform allows for a phase modulation and the addition of half-cycles. The need to include four (a_p, T_p, φ and γ) rather than two (a_p, T_p) parameters in the mathematical expression of a single wavelike function to characterize the coherent pulse of a pulse-like record has been voiced and addressed by Mavroeidis and Papageorgiou (2003). Their proposed elementary wavelike function that approximates the coherent velocity pulse of a pulse-like record is the product of a harmonic oscillation with an elevated cosine function,

$$v(t) = \frac{1}{2}\left(1 + \cos\left(\frac{2\pi f_p}{\gamma} t\right)\right)\cos(2\pi f_p + \varphi) \tag{10}$$

In equation (10), $f_p = 1/T_p$, is the frequency, φ is the phase and γ is the number of half-cycles of the wavelike function. Equation (10) is a slight modification of the Gabor (1946) "elementary" signal in which the harmonic oscillation (last term in equation 10) was multiplied with a Gaussian envelop. Both the Gabor (1946) "elementary" signal and the wavelike function given by equation (10) do not always have a zero mean; therefore, they are not wavelets with the context of the wavelet transform where the wavelet function needs to have finite energy and zero mean. Nevertheless, the time derivative of equation (10) is a zero mean signal and it has been defined as the Mavroeidis and Papageorgiou (M&P) wavelet

$$\psi\left(\frac{t-\xi}{s}, \varphi, \gamma\right) = \left(\sin\left(\frac{2\pi}{s\gamma}(t-\xi)\right)\cos\left(\frac{2\pi}{s}(t-\xi)+\varphi\right) + \gamma\sin\left(\frac{2\pi}{s}(t-\xi)+\varphi\right)\right)\left(1+\cos\left(\frac{2\pi}{s\gamma}(t-\xi)\right)\right) \tag{11}$$

In equation (11), the scale s, of the M&P wavelet is merely the period of the wavelet $s = T_p = 1/f_p$.

In this work, in addition to the records shown in Figures 4 and 14, four additional strong pulse-like records are used in the response analysis of the free-standing columns. They are all listed in

Table 1 together with their corresponding parameters a_p, T_p, φ and γ of the dominant, coherent acceleration pulse as they result from the Vassiliou and Makris (2011) extended wavelet transform. The four additional acceleration records from the 1971 San Fernando, 1983 Coalinga, 1992 Erzincan and 2004 Parkfield earthquakes are shown in Figure 15 together with their best matching wavelets.

Figure 16 plots the rotation and angular velocity time histories at the verge of overturning of the two free-standing columns shown when excited by the amplified horizontal-NS (left) and the horizontal-NS and vertical component (right) of the ground motions recorded during the 1992 Erzincan, Turkey earthquake. Figure 16 confirms that for longer duration pulses, rocking columns rotate slower and develop a relatively feeble rotational acceleration. In this case (which for very long duration pulses asymptotically tends to a quasi-static loading) slenderness dominates over size.

Figure 17 summarizes the amplified acceleration levels (overturning seismic coefficient, ε) due to a horizontal ground acceleration alone (h) or a combined horizontal and vertical ground acceleration ($h+v$) of the eight strong records considered in this study which are needed to overturn: (a) the monolithic column from Temple of Apollo, Syracuse, Italy ($2b = 2.0m$, $2h = 7.98m$, $\tan\alpha = 0.252$); and (b) a twice as tall column with the same base, $2b = 2.0m$ and height, $2h = 16m$ ($\tan\alpha = 0.252$). Figure 17 reveals that when the overturning seismic coefficient, ε, is ordered as a function of the peak horizontal ground acceleration of the records, the results do not exhibit any trend. This is because while a recorded ground motion may exhibit a high peak ground acceleration (see for instance the Pacoima Dam record from 1971 San Fernando earthquake shown in Figure 15), the column overturns due to a longer duration, destructive, coherent pulse (Bertero et al. 1978).

Analysis at the Limit State (Verge of Overturning)

Figure 17 clearly indicates that the peak-ground acceleration is a poor intensity measure to access the overturning potential of strong pulse-like ground motions. This is because the overturning potential of pulse-like ground motion depends not only on the amplitude of the acceleration pulse, a_p, but even more so, on the duration of the acceleration, T_p which influences the seismic displacement demand with its second power. Accordingly, the overturning potential of pulse-like ground motions is expressed in this work with the energetic length scale of the pulse $= L_e = a_p T_p^{\ 2}$ (Makris and Black 2004a,b, Vassiliou and Makris 2011).

Figure 18 plots the same results shown in Figure 17 which are now ordered as a function of the energetic length scale of the dominant coherent pulse of the record, $L_e = a_p T_p^{\ 2}$ (see Table 1). The first observation is that, while there is some scattering (due to some high-frequency spikes), the seismic coefficient $\varepsilon = \ddot{u}_g^{\ overt} / g$, needed to create overturning is a decreasing function of the length scale of the coherent acceleration pulse, L_e.Furthermore, Figure 18 shows that for larger values of L_e (say $L_e > 5m$) –that is for longer duration pulses, a shorter column is more stable than the equal-base taller column (slenderness prevails over size). In contrast, for lower values of L_e (say $L_e < 4m$) –that is for shorter duration pulses; therefore, there is a more vivid engagement of the rotational inertia of the column (Makris 2014), the results are mixed and there are situations where size prevails over slenderness.

Within the context of a capacity design framework and with reference to Figure 19, the limit state of a free-standing rocking column is reached when during ground shaking its rotation, θ reaches its slenderness, α–that is when the center of gravity is above the pivot point. Accordingly, within the context of capacity design, the displacement capacity of a free-standing rocking column is merely,

$$u_{\max} = R\sin\alpha = b \tag{12}$$

Equation (12), while very simple, shows in a primitive; yet direct way that the seismic capacity of a slender free-standing column is the product of the two competing size parameters; the size, R, and the slenderness, α. It essentially indicates that the seismic stability of a tall, free-standing column depends directly on its base-width $= 2b = 2R\sin\alpha$ rather than solely on the size, R, or solely on the slenderness, α, of the column.

In view of the result offered by equation (12), the overturning seismic coefficient, ε, needs to be expressed as a function of the length scale of the dominant coherent pulse of the record, $L_e = a_p T_p^{\,2}$, normalized to the displacement capacity of the free-standing column, $b = R\sin\alpha$. Accordingly, we introduce the overturning potential index, $\lambda = \dfrac{L_e}{b} = \dfrac{a_p T_p^{\,2}}{R\sin\alpha}$, to express the overturning potential of a pulse-like ground motion with acceleration amplitude, a_p, and duration, T_p, on a tall free-standing column with any height and any slenderness and base width $= 2b$. The practical value of the overturning potential index, $\lambda = L_e / b$, is illustrated in Figure 20 which in addition to the results presented in Figure 18 it plots the overturning seismic coefficients, ε, which are needed to overturn the remaining columns shown in Figure 2 with bases $2b = 1.0m$ and

$2b = 4.0m$.

Figure 20 reveals that the seismic coefficient, $\varepsilon = \ddot{u}_g^{overt.} / g$ that is needed to overturn a tall column of any size and any slenderness is a decreasing function of the overturning potential index, $\lambda = L_e / b$. When $\lambda \geq 10$ any tall, free-standing column most likely overturns. Furthermore, Figure 20 indicates that while a tall, slender column will uplift when the seismic coefficient exceeds the slenderness ($\varepsilon > \tan\alpha$), the overturning seismic coefficient assumes very large values indicating that tall, physically realizable, free-standing columns are most stable under earthquake shaking.

On the other hand, the finding from Figure 20, that when $\lambda \geq 10$ any tall, free-standing column most likely overturns, is valid provided that the peak-ground acceleration (PGA) of the ground shaking is capable to induce uplifting ($PGA > g\tan\alpha$). It is worth mentioning that some, otherwise devastating, ground motions such as the recent Lamjung-90 record from the 2015 Nepal earthquake shown in Figure 21 (bottom) may exhibit very long pulse durations, yet, relatively low ground accelerations. Given that the Lamjung-90 record has a $PGA = 0.16g$, any column with $\tan\alpha < 0.16$, upon uplifting will also overturn given the very long duration of the dominant pulse ($T_p \approx 5.0s$). Figure 21 (top) shows that the $2.00m \times 16.00m$ column ($\tan\alpha = 1/8 = 0.125$), upon uplifting immediately overturns when subjected to the Lamjung-90 record given that $L_e = \dfrac{a_p T_p^{\ 2}}{b} = 38.27$.

Conclusions

This paper investigates how the seismic stability of a free-standing column is affected when its height increases while its width is kept constant. When a column with a given base becomes taller and taller there is a competition between the increase in the size of the column (more stable) and the increase in its slenderness (less stable); and the paper concludes that the outcome of this competition is sensitive to the local details and the frequency of the predominant coherent pulse of the excitation.

When a free-standing column is excited by a single-frequency mathematical pulse excitations two opposite trends are identified: (a) in the event of a long duration pulse with a slowly increasing ground acceleration, upon the column uplifts ($\ddot{u}_g(t) > g\tan\alpha$) the engagement of the rotational inertia of the column (proportional to R^2) is feeble; and in this case the slenderness has a dominant effect over size; and (b) in the event of a shorter duration pulse (more high-frequency pulse), the free-standing column experiences appreciable rotational accelerations which engage vividly the rotational inertia of the column (proportional to R^2) and in this case the increase of the size offsets the effects due to the increase of the slenderness.

The increase in the stability due to increase in height may be further enhanced due to a sudden transition from the lower mode of overturning with impact to the higher mode of overturning without impact. Because of this bifurcation phenomenon a tall and slender column (which can only overturn without impact) may be appreciably more stable than a much shorter column with the same base (which can overturn with impact -see Figure 7-). In the event of a recorded earthquake ground motion that contains several frequencies the abovementioned enhanced stability of a taller column is harder to observe; nevertheless, it may happen as shown in Figures 12 and 13.

The paper confirms an observation that has been reported in the literature for more than three decades (yet it has not received the attention it deserves) –that the vertical ground acceleration has a marginal effect on the stability of a free-standing column. This is primarily because the vertical ground acceleration enters the equation of motion after being multiplied with $\sin[\alpha - \theta(t)] << 1$; whereas, the horizontal acceleration enters the equation of motion after being multiplied with $\cos[\alpha - \theta(t)] \approx 1.0$.

Finally the paper concludes that the level of ground shaking that is needed to overturn a tall, free-standing column of any size and any slenderness is a decreasing function of the length scale, $a_p T_p^{\ 2}$, of the dominant, coherent acceleration pulse normalized to the base-width of the column.

Data and Resources

The accelerograph data used in this study are from the Pacific Earthquake Engineering Research Center (PEER) strong ground motion database at http://peer.berkeley.edu (last accessed September 2011) and from the Center for Engineering Strong Motion Data database (USGS-CGS) at http://strongmotioncenter.org/ (last accessed November 2015).

Acknowledgements

Partial financial support for this study has been provided by the research project "SeismoRockBridge," Number 2295, which is implemented under the "ARISTEIA" Action of the "Operational Program Education and Lifelong Learning" and is cofunded by the European Social Fund (ESF) and Greek National Resources.

References

Abrahamson, N., (2001). Incorporating effects of near fault tectonic deformation into design ground motions, MCEER & CSEE Department's Seminar Series, SUNY Buffalo, New York.

Alavi B., and H. Krawinkler (2001). Effects of near-source ground motions on frame-structures, Technical Report No. 138, The John A. Blume Earthquake Engineering Center, Stanford University.

Baker W.J. (2007). Quantitative classification of near fault ground motions using wavelet analysis, *Bull Seism Soc Am* **97** 1486–1501.

Barenblatt, G.I. (1996). *Scaling, self-similarity, and intermediate asymptotics*, Cambridge Texts in Applied Mathematics, Cambridge University Press: Cambridge, UK.

Bertero V.V., S.A. Mahin and R.A. Herrera (1976). Aseismic design implications of near-fault san Fernando earthquake records, *Earthquake Engineering and Structural Dynamics* **6** 31–42.

Bolt B.A. (1976). Abnormal Seismology, *Bull Seism Soc Am* **66** 617-623.

Dinsmoor W.B. (1975). *The Architecture of Ancient Greece*. W.W. Norton & Company,Inc: New York.

Fletcher B. (2001). *A History of Architecture on the Comparative Method*, Elsevier Science & Technology.

Hall J.F., T.H. Heaton, M.W. Halling and D.J. Wald. Near-source ground motion and its effects on flexible buildings, *Earthquake Spectra* **11**(4) 569–605.

Housner G.W. (1963). The behavior of inverted pendulum structures during earthquakes, *Bull. Seism. Soc. Am.* **53**(2) 404–417.

Ishiyama Y. (1982). Motions of Rigid Bodies and Criteria for Overturning by Earthquake Excitations, *Earthquake Engineering and Structural Dynamics* **10** 635–650.

Kirkpatrick, P. (1927). Seismic measurements by the overthrow of columns, *Bull. Seismol. Soc. Am.* **17**, 95–109.

Karavasilis T.L., N. Makris, N. Bazeos and D.E. Beskos (2010). Dimensional response analysis of multistory regular steel MRF subjected to pulselike earthquake ground motions, *Journal of Structural Engineering* **136**(8) 921–932.

Konstantinidis, D., and N. Makris (2005). Seismic response analysis of multidrum classical columns, *Earthquake Engineering and Structural Dynamics* **34**, 1243–1270.

Makris N. (1997). Rigidity–plasticity–viscosity: can electrorheological dampers protect base-isolated structures from near-source ground motions?, *Earthquake Engineering and Structural Dynamics* **26** 571–591.

Makris N. (2014). The Role of the Rotational Inertia on the Seismic Resistance of Free-Standing Rocking Columns and Articulated Frames, *Bull. Seism. Soc. Am.* **104** 2226–2239.

Makris N, and C.J. Black (2004a). Dimensional analysis of rigid-plastic and elastoplastic structures under pulse-type excitations, *Journal of Engineering Mechanics* ASCE **130**(9) 1006–1018.

Makris N, and C.J. Black (2004b). Dimensional analysis of bilinear oscillators under pulse-type excitations. *Journal of Engineering Mechanics* ASCE **130**(9) 1019–1031.

Makris, and S.P. Chang (2000a). Response of Damped Oscillators to Cyclical Pulses, *Journal of Engineering Mechanics ASCE* **126**(2) 123-131.

Makris N and S-P Chang (2000b). Effect of viscous, viscoplastic and friction damping on the response of seismic isolated structures, *Earthquake Engineering and Structural Dynamics* **29**(1) 85–107.

Makris N. and C. Psychogios (2006). Dimensional response analysis of yielding structures with first-mode dominated response, *Earthquake Engineering and Structural Dynamics* **35** 1203–1224.

Makris N. and M.F. Vassiliou (2012). Sizing the Slenderness of free-standing rocking columns to withstand earthquake shaking , *Archive of Applied Mechanics* **82** 1497-1511.

Makris N. and M.F. Vassiliou (2014). Are Some Top-Heavy Structures More Stable?, *Journal of Structural Engineering, ASCE* DOI: 10.1061/(ASCE)ST.1943-541X.0000933.

Mark IS (1993). The Sanctuary of Athena Nike in Athens: Architectural Stages and Chronology, *The American School of Classical Studies at Athens* **26** 1-185.

Mavroeidis G.P. and A.S. Papageorgiou (2003). A mathematical representation of near-fault ground motions, *Bull. Seism. Soc. Am.* **93**(3) 1099–1131.

Powell B. (1905). The Temple of Apollo Corinth, *American Journal of Archaeology* **9**(1) 44-63.

Ricker N. (1943). Further developments in the wavelet theory of seismogram structure, *Bull. Seism. Soc. Am*, **33** 197–228.

Ricker N. (1944). Wavelet functions and their polynomials, *Geophysics* **9** 314–323.

Singh J.P. (1985). Earthquake ground motions: Implications for designing structures and reconciling structural damage, *Earthquake Spectra* **1** 239:270**.**

Somerville P. and R. Graves (1993). Conditions that give rise to unusually large long period ground motions, *Struct Design Tall Buildings* **2** 211–232.

Somerville P. (1998). Development of an improved representation of near-fault ground motions, SMIP98-CDMG Oakland CA 1–20.

Taniguchi T. (2002). Non-linear response analyses of rectangular rigid bodies subjected to horizontal and vertical ground motion, *Earthquake Engineering and Structural Dynamics* **31** 1481–1500.

Vassiliou M.F., and N. Makris (2011). Estimating time scales and length scales in pulse-like earthquake acceleration records with wavelet analysis, *Bull. Seism. Soc. Am.* **101**(2) 596–618.

Veletsos A.S., N.M. Newmark, and C.V. Chelepati (1965). Deformation spectra for elastic and elastoplastic systems subjected to ground shock and earthquake motions, *Proceedings of the 3rd World Conference on Earthquake Engineering*, vol. II, Wellington, New Zealand, 663–682.

Yim C.S., A.K. Chopra and J. Penzien (1980). Rocking response of rigid blocks to earthquakes, *Earthquake Engineering and Structural Dynamics* **8**(6) 565–587.

Zhang J. and N. Makris (2001). Rocking response of free-standing blocks under cycloidal pulses, *Journal of Engineering Mechanics (ASCE)* **127**(5) 473–483.

Table 1. Information pertinent to the strong records used in this study together with the parameters of the best matching wavelet of their dominant, coherent acceleration pulse.

Earthquake	**Record**	**Magnitude** M_W	**Epicentral Distance** km	$PGA(g)$	$a_p(g)$	$T_p(s)$	φ	γ	$L_e(m)$
1971 San Fernando	Pacoima Dam/164	6.6	11.9	1.23	0.3	1.35	0	3	5.36
1979 Coyote Lake	Gilroy Array #6/230	5.74	3.11	0.42	0.35	1.00	0	1	3.43
1983 Coalinga	Transmitter Hill/270	5.18	10.03	0.78	0.46	0.80	0.79	1.5	2.89
1986 San Salvador	Geotech Inv. Center/090	5.4	4.3	0.70	0.45	0.70	0	3	2.16
1986 San Salvador	Geotech Inv. Center/180	5.4	4.3	0.42	0.45	0.80	0	3	2.83
1992 Erzincan	Erzincan/NS	6.9	13.0	0.52	0.34	1.55	1.57	1	8.01
1995 Kobe	Takarazuke/000	6.9	1.2	0.70	0.49	1.15	1.57	1	6.36
2004 Parkfield	Cholame#2/360	6.0	3.01	0.37	0.40	0.90	2.36	1.5	3.49

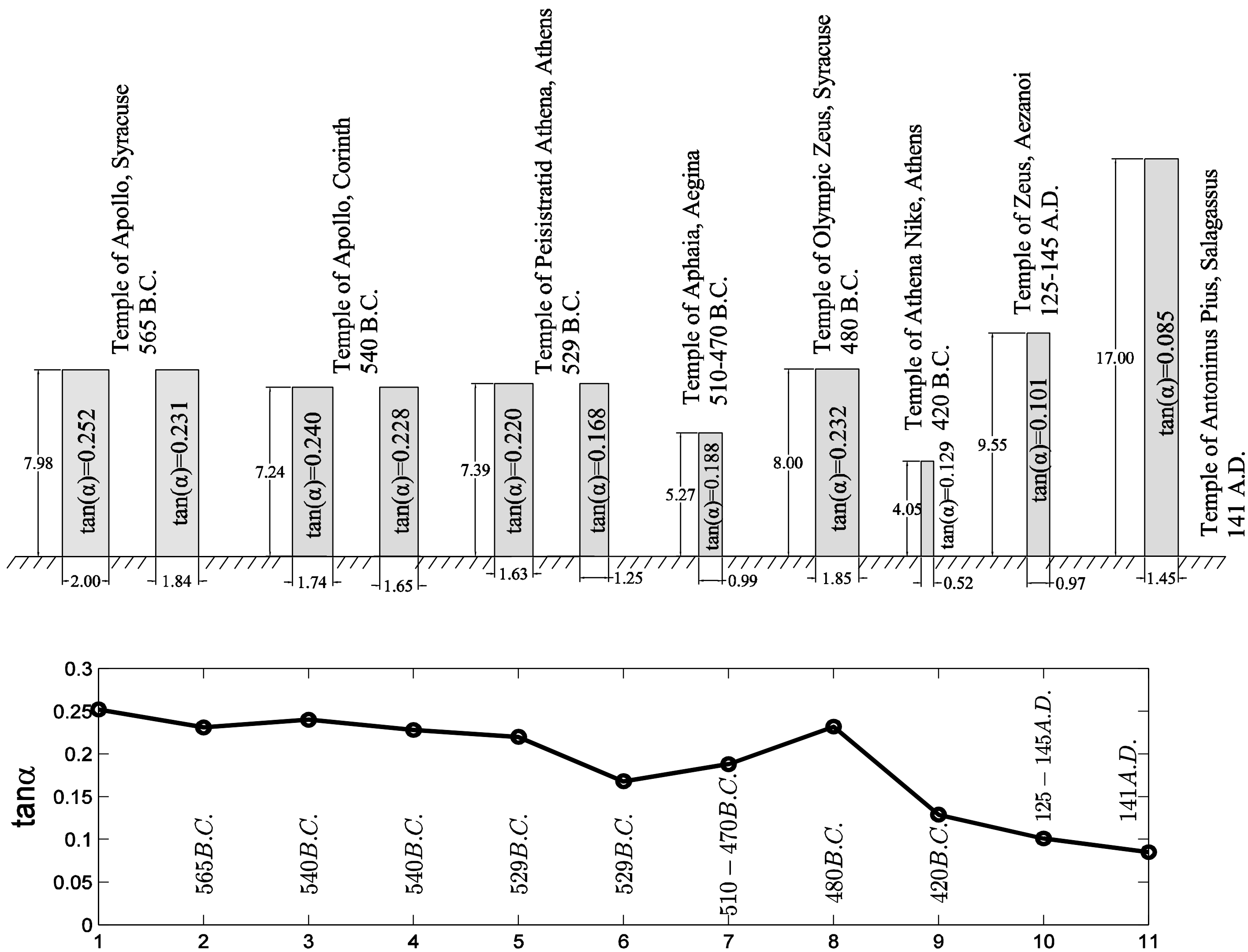

Figure 1. Top: Dimensions in meters of selected monolithic ancient columns in chronological order (Dinsmoor 1975; Fletcher 2001); Bottom: The corresponding slenderness values of the columns shown above. A free-standing column uplifts when the ground acceleration exceeds $g \tan \alpha$.

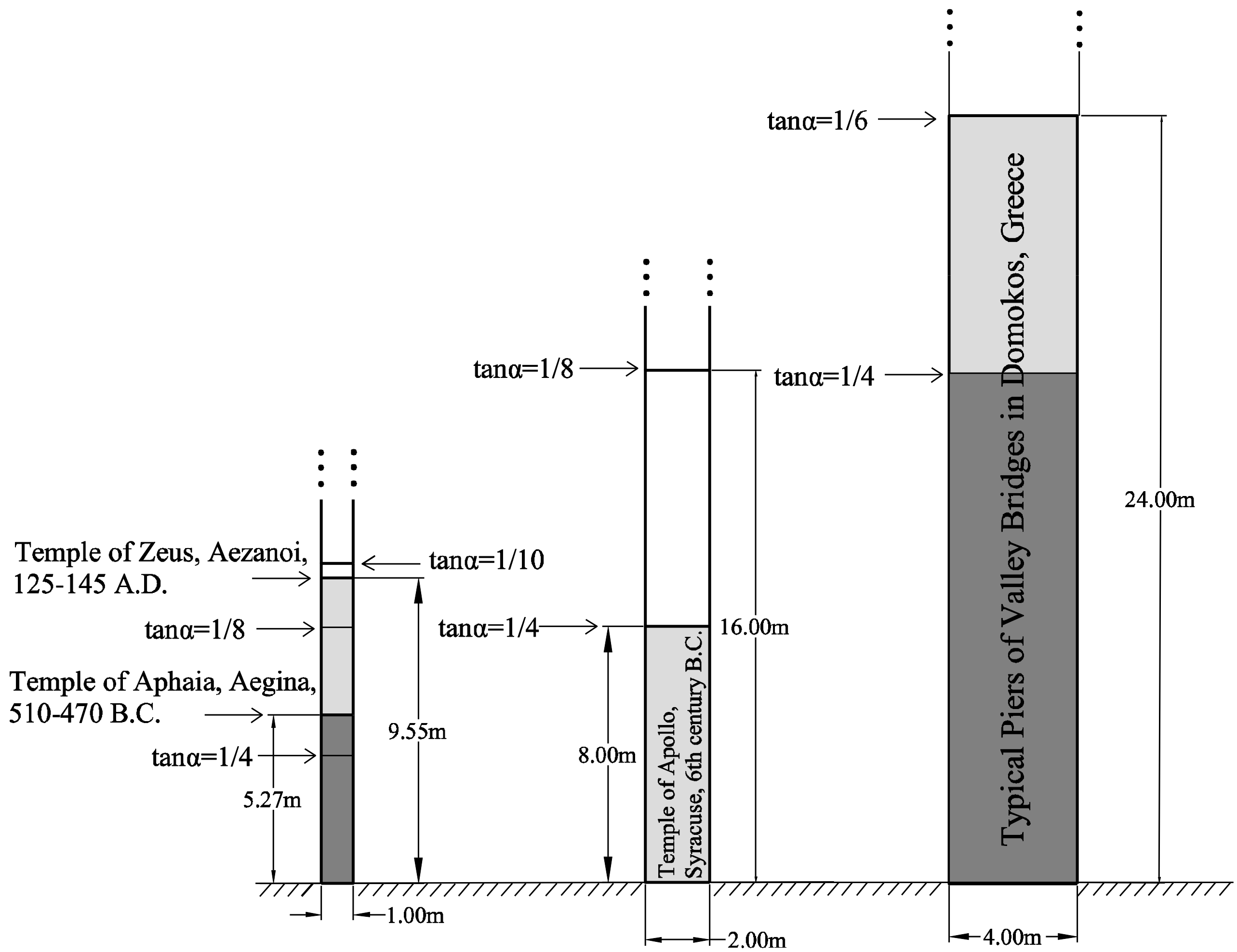

Figure 2. The three columns studied in this paper with constant width $2b = 1.0m$, $2.0m$ and $4.0m$; and increasing size.

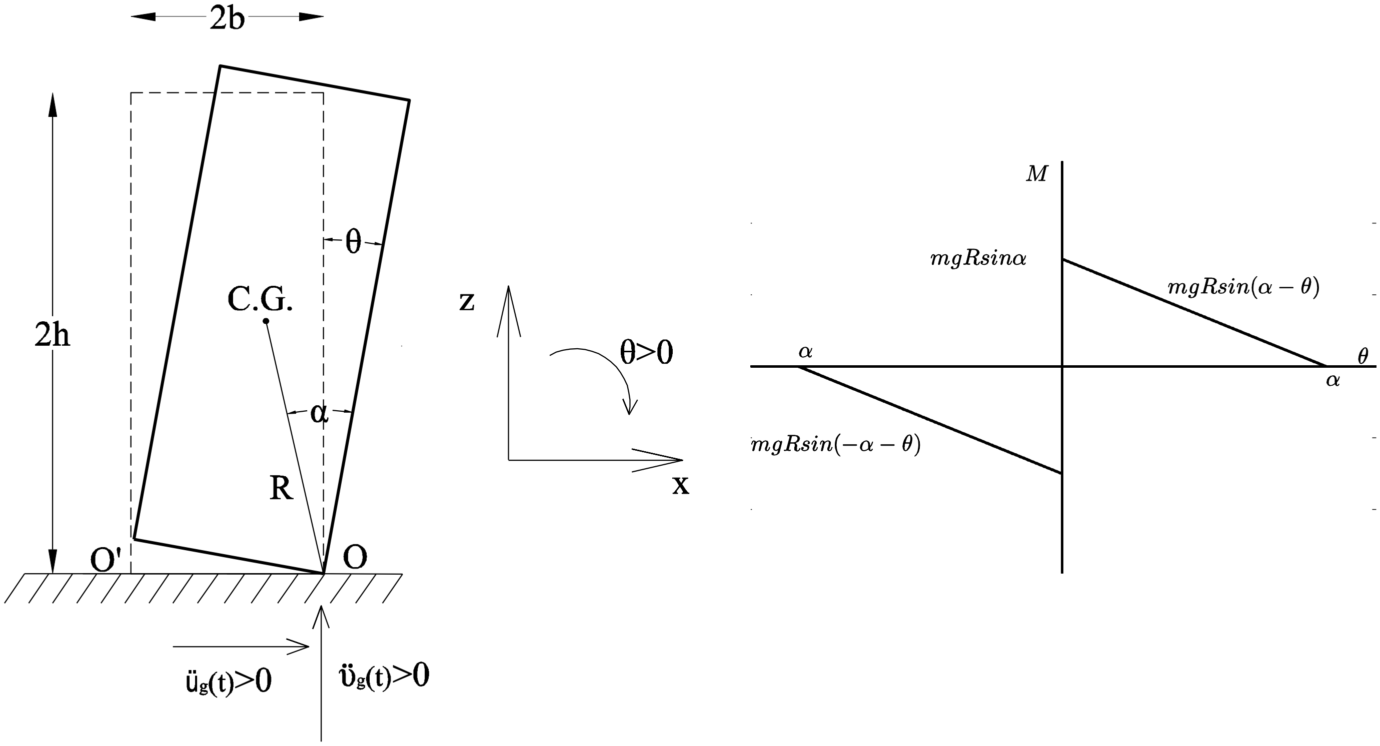

Figure 3. Left: Geometric characteristics of the free-standing column. Right: Moment-rotation diagram of a rocking column.

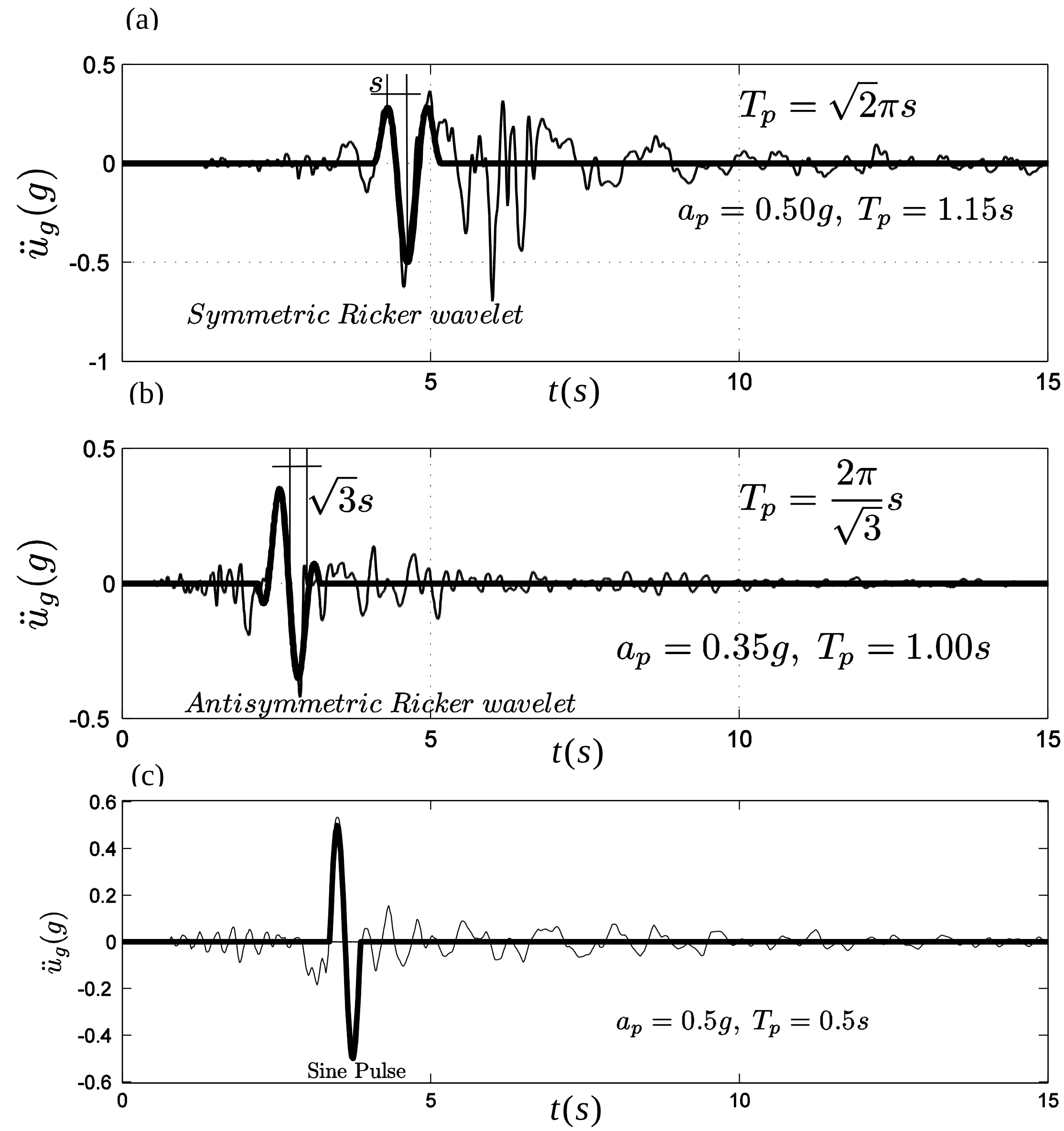

Figure 4. Acceleration time histories recorded during (a) the 1995 Kobe, Japan earthquake -NS component of the Takarazuka record, together with a symmetric Ricker wavelet; (b) the 1979 Coyote Lake, California earthquake –fault normal component of Gilroy Array#6 record, together with an antisymmetric Ricker wavelet; (c) the 1973 Lefkada, Greece earthquake –OTE record, together with a one-cycle sine pulse.

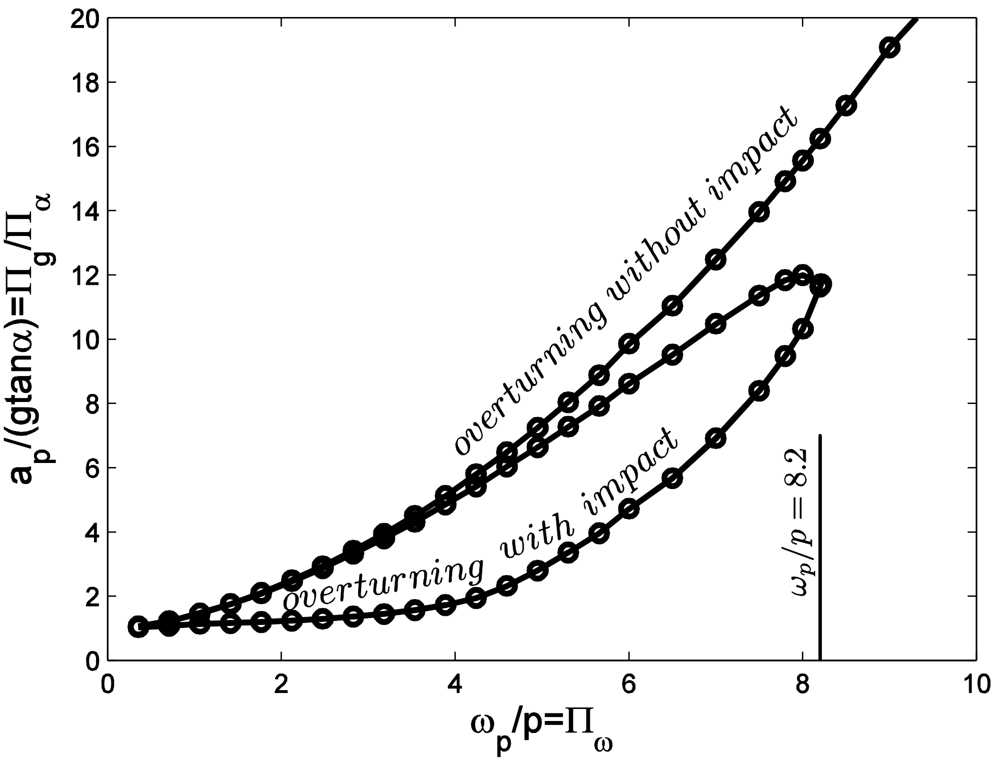

Short columns
or low-frequency pulses

Large columns
or high-frequency pulses

Figure 5. Overturning acceleration spectrum of the free-standing rocking column with $\tan\alpha = 0.25$ when is subjected to a one-sine acceleration pulse, Lower overturning boundary: overturning with one impact (mode I); Higher overturning boundary: overturning without impact (mode II). For this given slenderness $\tan\alpha = 0.25$, whenever $\omega_p / p > 8.2$ the free-standing column overturns only without impact (mode II).

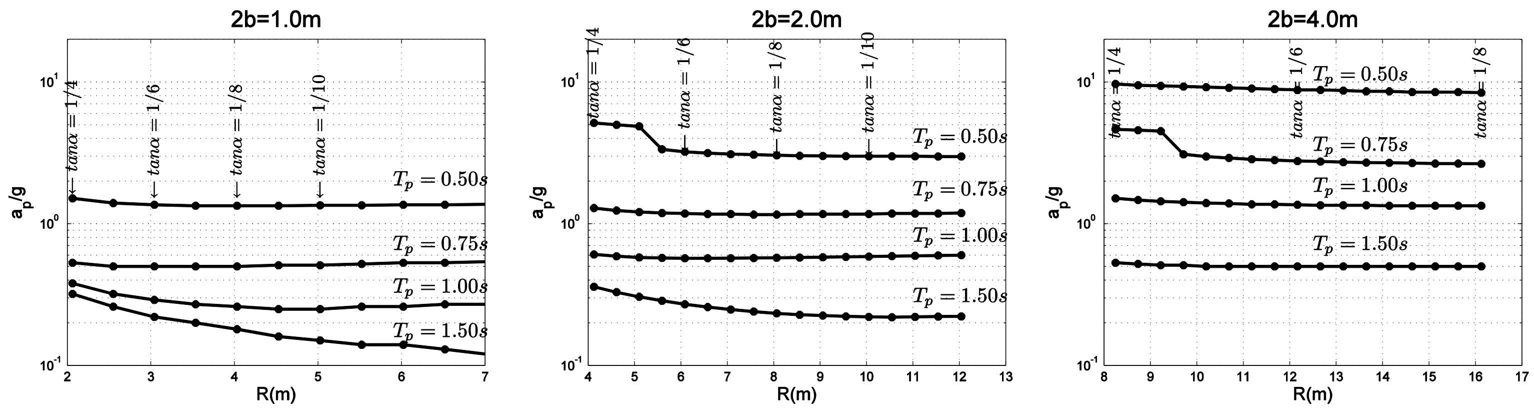

Figure 6. Overturning acceleration diagrams due to a one-sine pulse that is needed to overturn a free-standing column with base $2b = 1.0m$ (left), $2b = 2.0m$ (center), $2b = 4.0m$ (right).

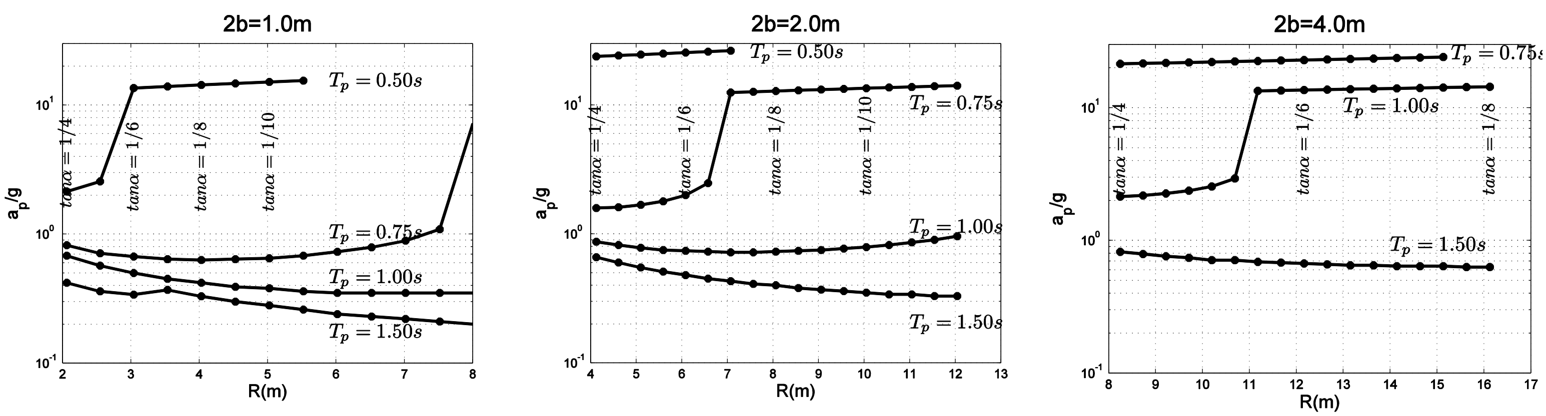

Figure 7. Overturning acceleration diagrams due to a symmetric Ricker pulse that is needed to overturn a free-standing column with base $2b = 1.0m$ (left), $2b = 2.0m$ (center), $2b = 4.0m$ (right). The sudden jumps in some diagrams as the size increases is because beyond a certain size the free-standing column can only overturn without impact (second mode of overturning); therefore, the need for an appreciable larger overturning acceleration amplitude.

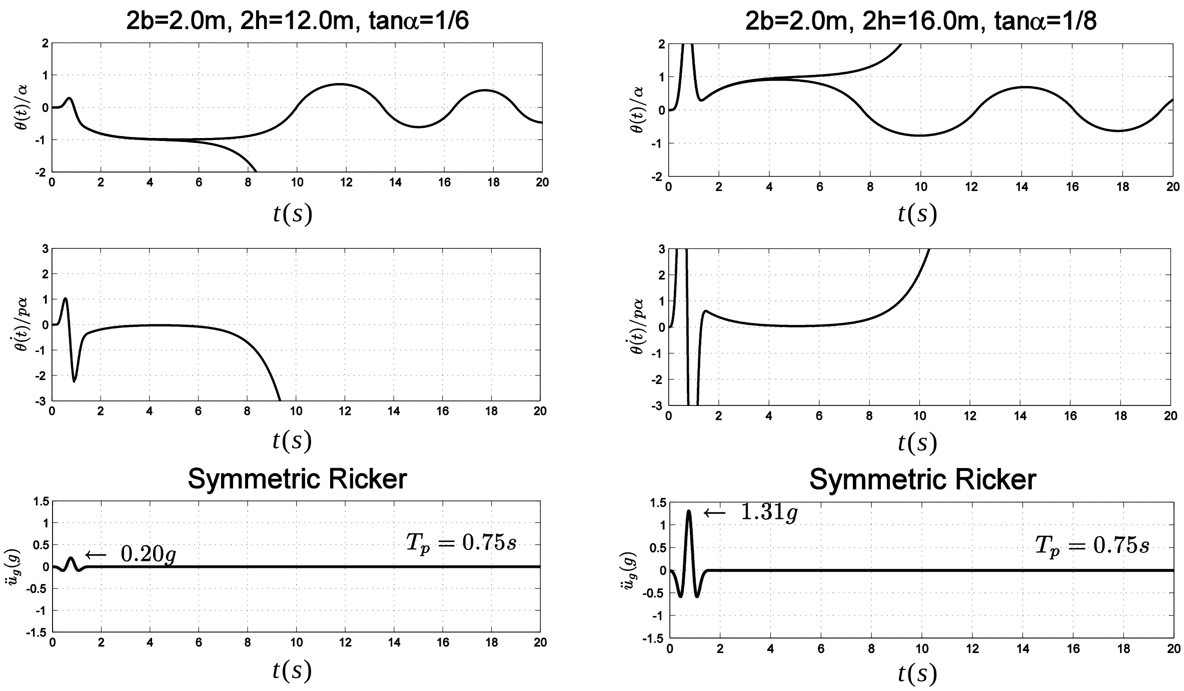

Figure 8. Rotation and angular velocity time histories of the two free-standing columns having width $2b = 2.0m$ and heights $2h = 12.0m$ (left) and $2h = 16.0m$ (right) when excited by a symmetric Ricker wavelet with duration $T_p = 0.75s$. The $12.0m$ column on the left overturns with one impact; whereas, the $16.0m$ column on the right can only overturn without impact when subjected to a much higher acceleration.

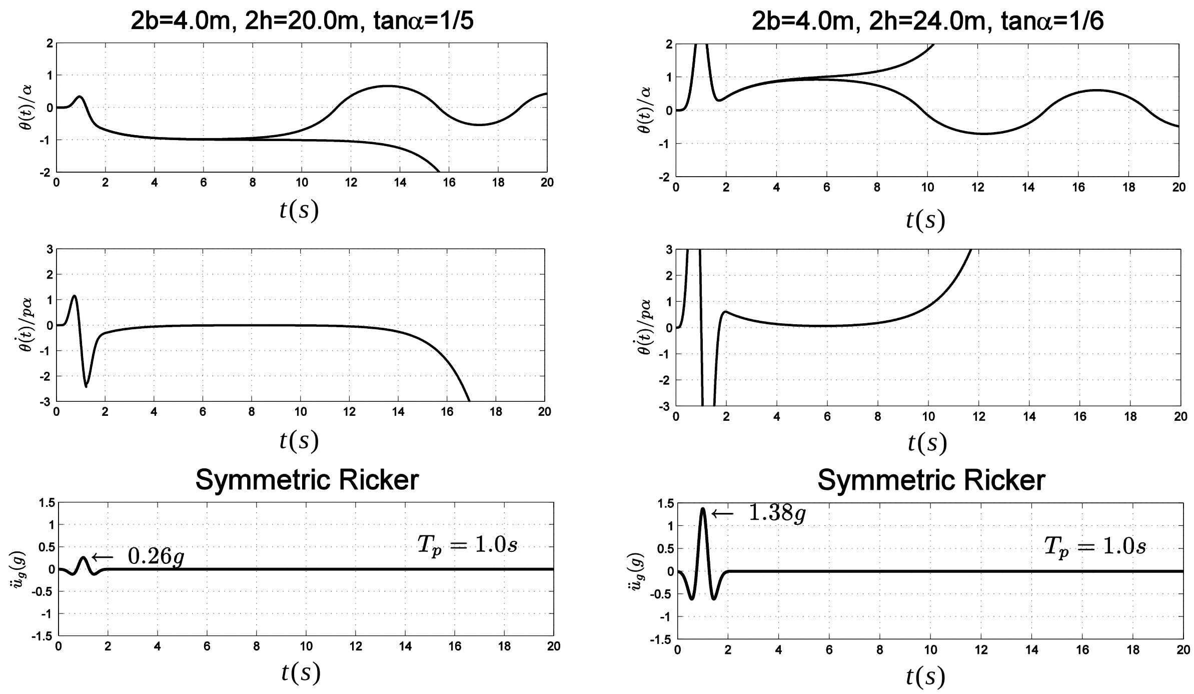

Figure 9. Rotation and angular velocity time histories of the two free-standing columns having width $2b = 4.0m$ and heights $2h = 20.0m$ (left) and $2h = 24.0m$ (right) when excited by a symmetric Ricker wavelet with duration $T_p = 1.0s$. The $20.0m$ column on the left overturns with one impact; whereas, the $24.0m$ column on the right can only overturn without impact when subjected to a much higher acceleration.

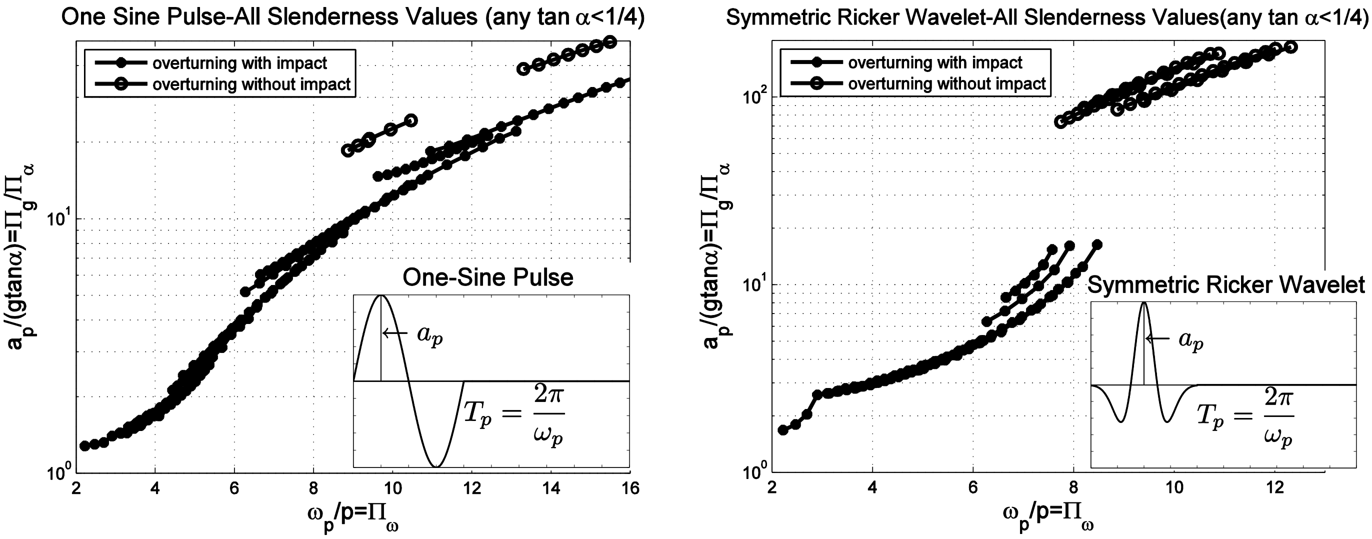

Figure 10. Overturning acceleration spectra due to a one-sine pulse (left) and a symmetric Ricker pulse (second derivative of the Gaussian -right). When the data presented in the three subplots show in each of the Figure 6 and 7 are plotted in terms of the dimensionless products appearing in equation (10) appreciable order emerges. The data however do not collapse to a single master curve because they are for various slenderness values (several Π_α terms).

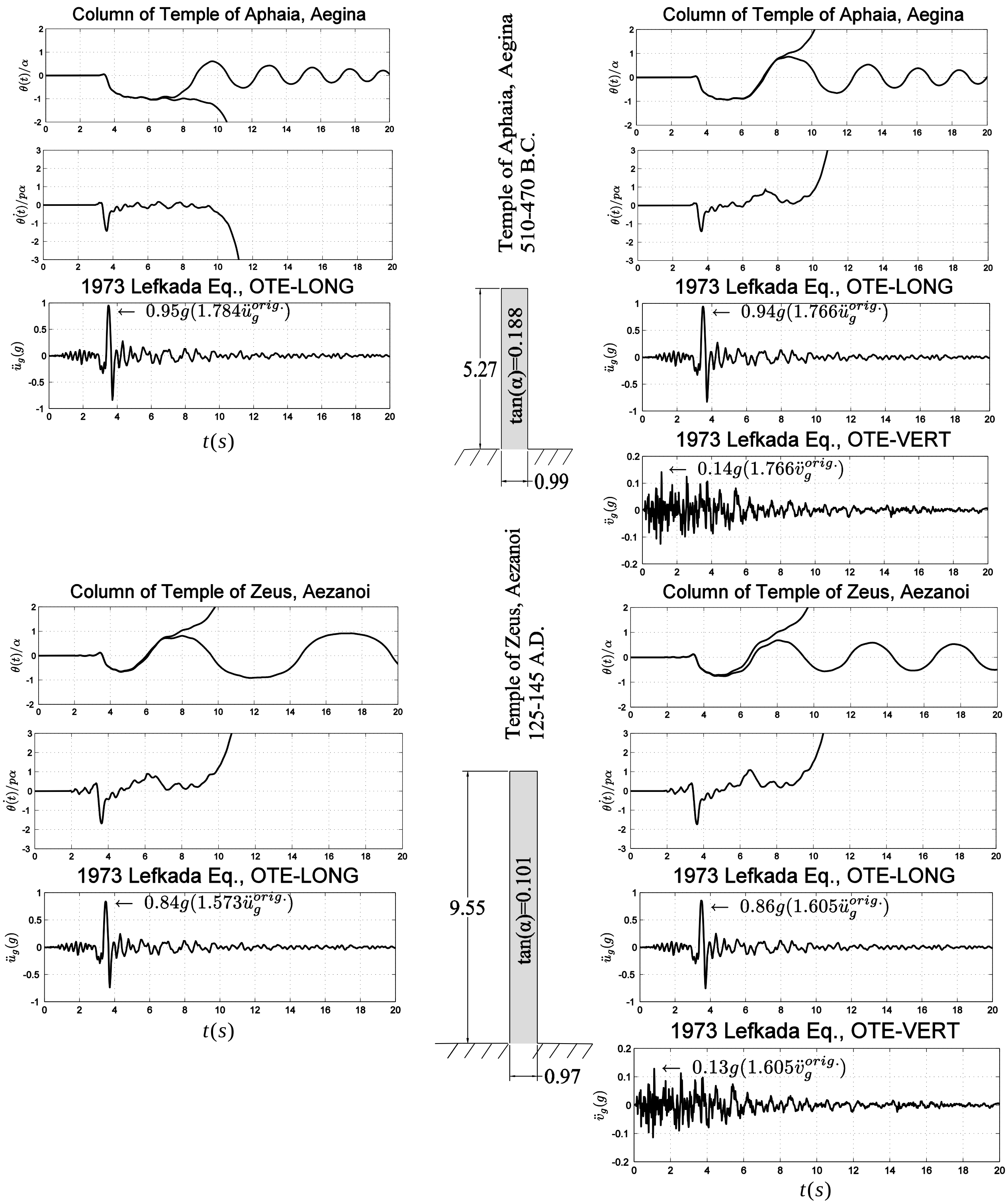

Figure 11. Rotation and angular velocity time histories at the verge of overturning of the columns from the Temples of Aphaia, Aegina, Greece (top) and Zeus, Aezanoi, Turkey (bottom) when excited by the amplified horizontal only (left) and the horizontal and vertical components (right) of the OTE ground motion recorded during the 1973 Lefkada, Greece earthquake.

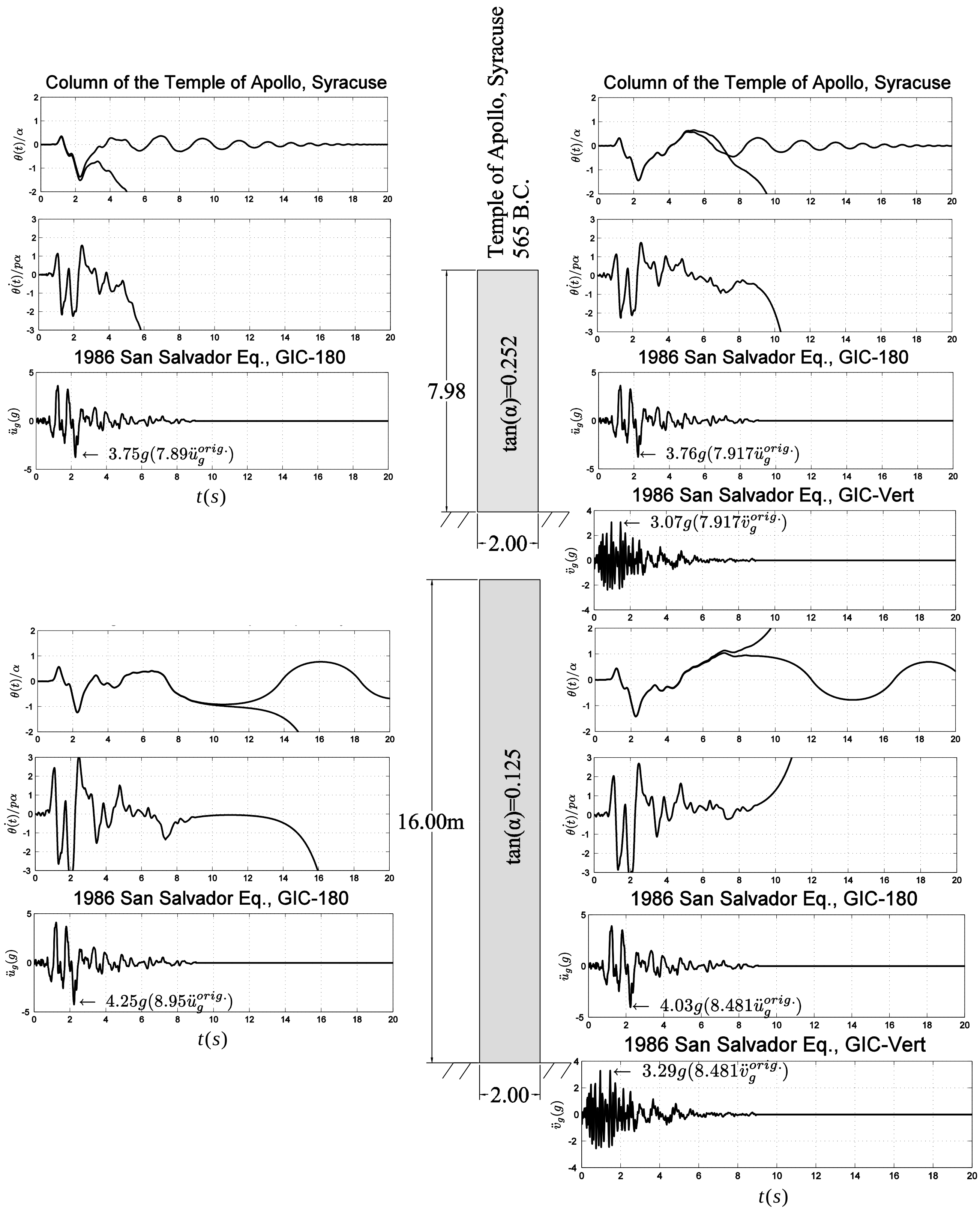

Figure 12. Rotation and angular velocity time histories at the verge of overturning of the columns from the Temple of Apollo, Syracuse, Italy (top) and taller column with twice the height and slenderness (bottom) when excited by the amplified horizontal only (left) and the horizontal and vertical components (right) of the GIC-180 ground motion recorded during the 1986 San Salvador earthquake.

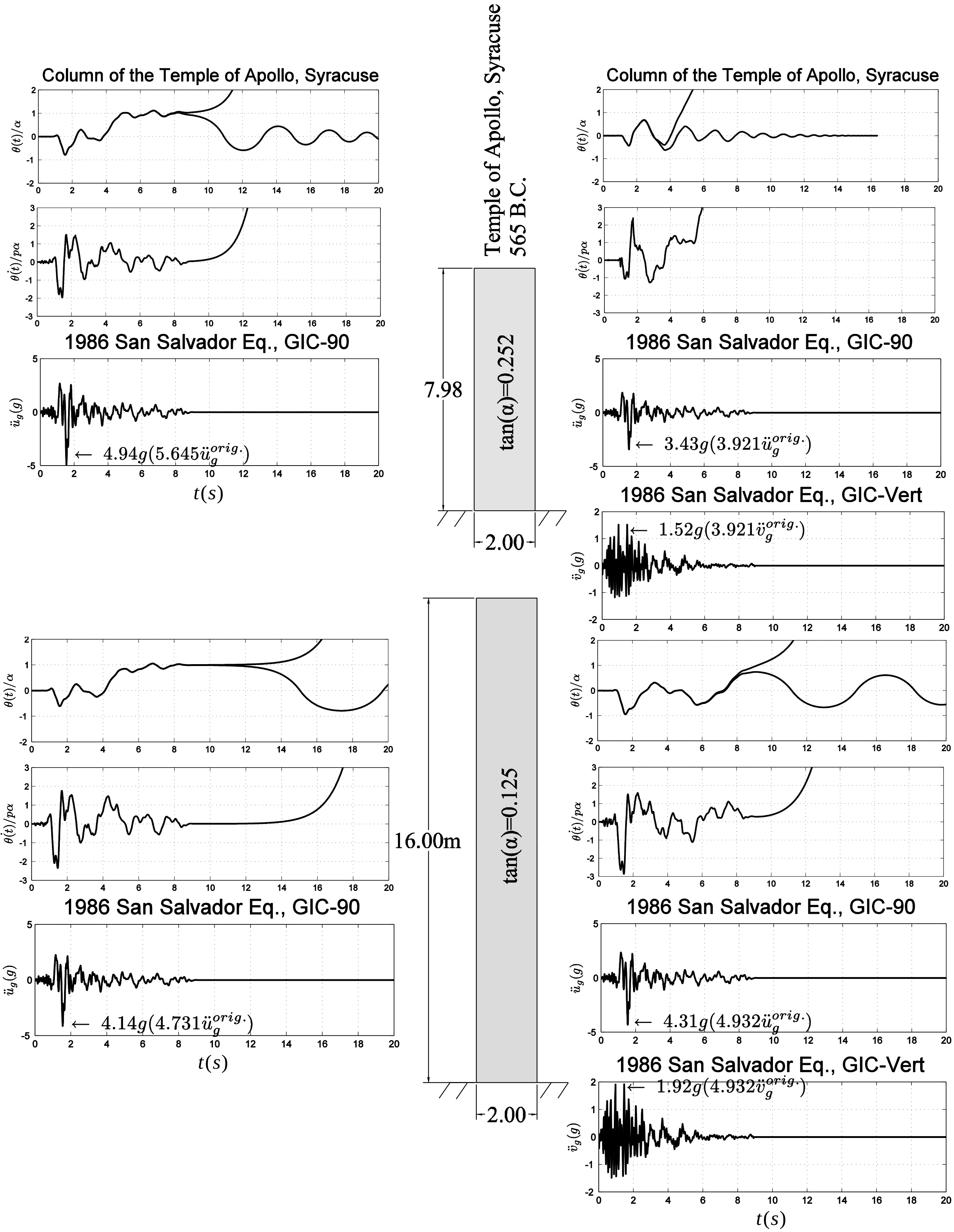

Figure 13. Rotation and angular velocity time histories at the verge of overturning of the columns from the Temple of Apollo, Syracuse, Italy (top) and taller column with twice the height and slenderness (bottom) when excited by the amplified horizontal only (left) and the horizontal and vertical components (right) of the GIC-90 ground motion recorded during the 1986 San Salvador earthquake.

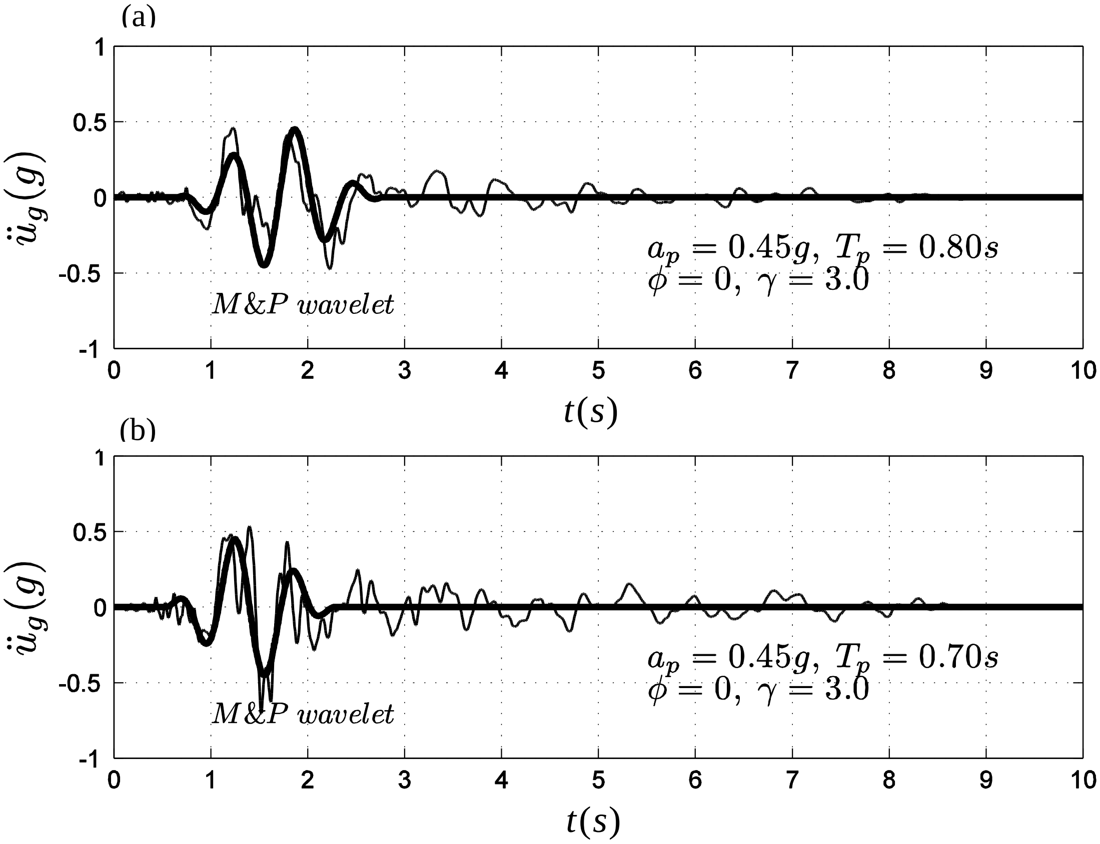

Figure 14. Acceleration time histories recorded during the 1986 San Salvador earthquake: (a) North-South, GIC-180 record; (b) East-West, GIC-90 record together with the best matching M&P wavelet (Vassiliou and Makris 2011).

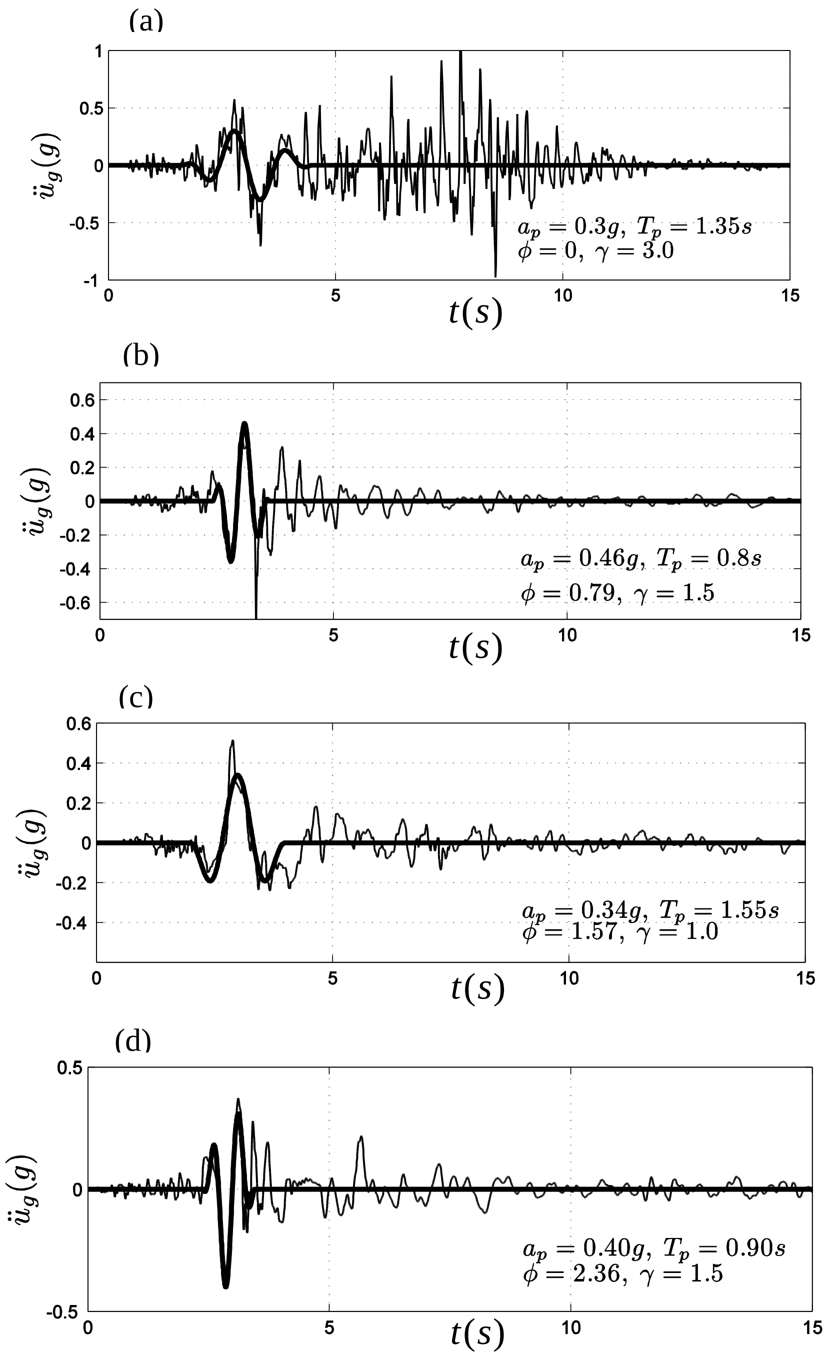

Figure 15. Acceleration time histories recorded during the (a) 1971 San Fernando earthquake – fault normal component of the Pacoima Dam record; (b) 1983 Coalinga earthquake –East-West component of the Transmitter Hill record; (c) North-South record from 1992 Erzincan, Turkey earthquake; (d) 2004 Parkfield earthquake –North-South component of the Cholame Array#2 record; together with their best matching M&P wavelets (Vassiliou and Makris 2011).

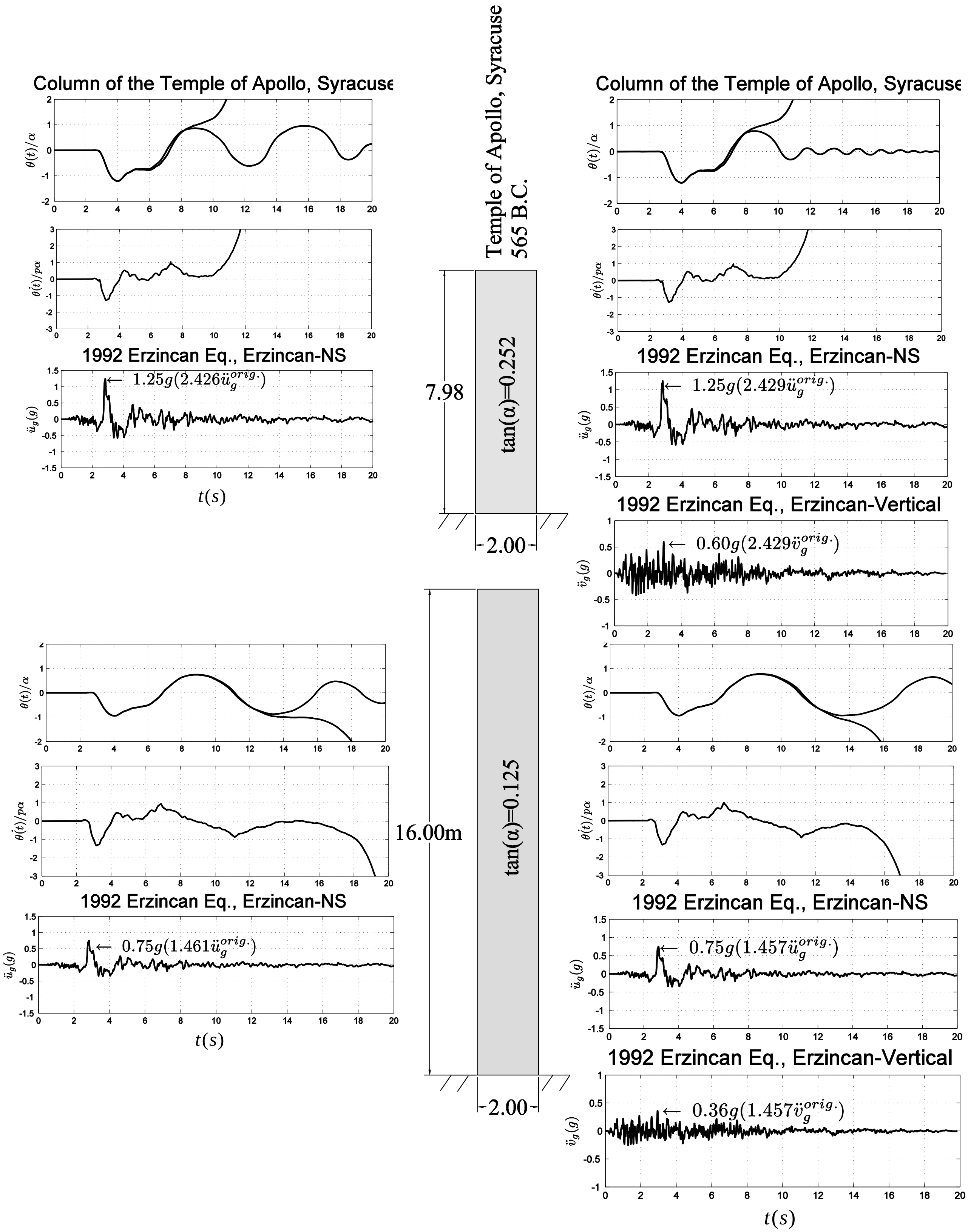

Figure 16. Rotation and angular velocity time histories at the verge of overturning of the columns from the Temple of Apollo, Syracuse, Italy (top) and taller column with twice the height and slenderness (bottom) when excited by the amplified horizontal only (left) and the horizontal and vertical components (right) of the 1992 Erzincan, Turkey earthquake.

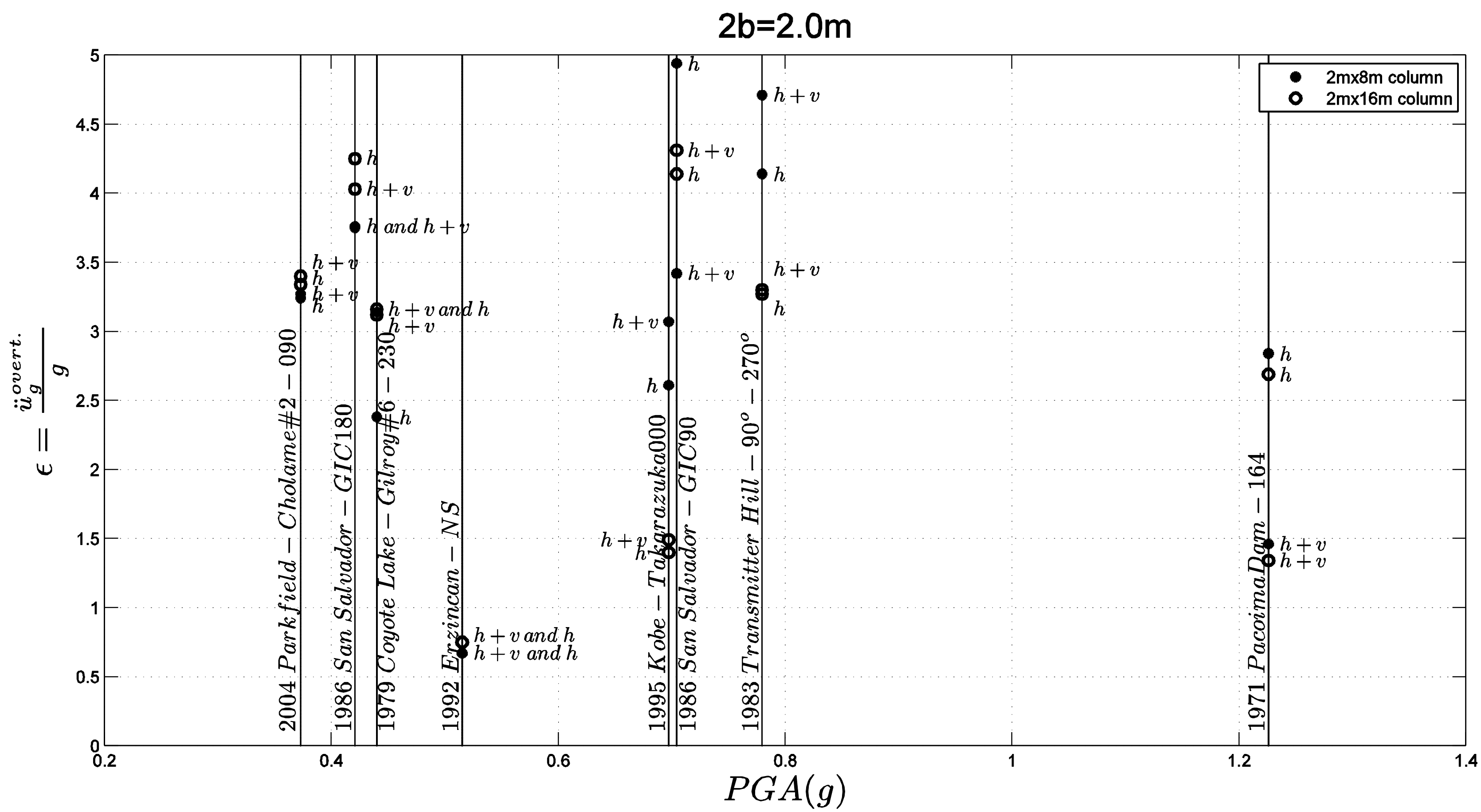

Figure 17. Overturning seismic coefficient, ε, of the amplified ground motions which are needed to overturn the monolithic column from the Temple of Apollo, Syracuse (dark dots) and a taller column with the same base $= 2.0m$ and twice the height (empty circles). In most case the effect of including the vertical acceleration ($h+v$) is marginal. The values of the overturning seismic coefficient, ε, are ordered with increasing peak horizontal ground acceleration of the records. The results are scattered without exhibiting any trend.

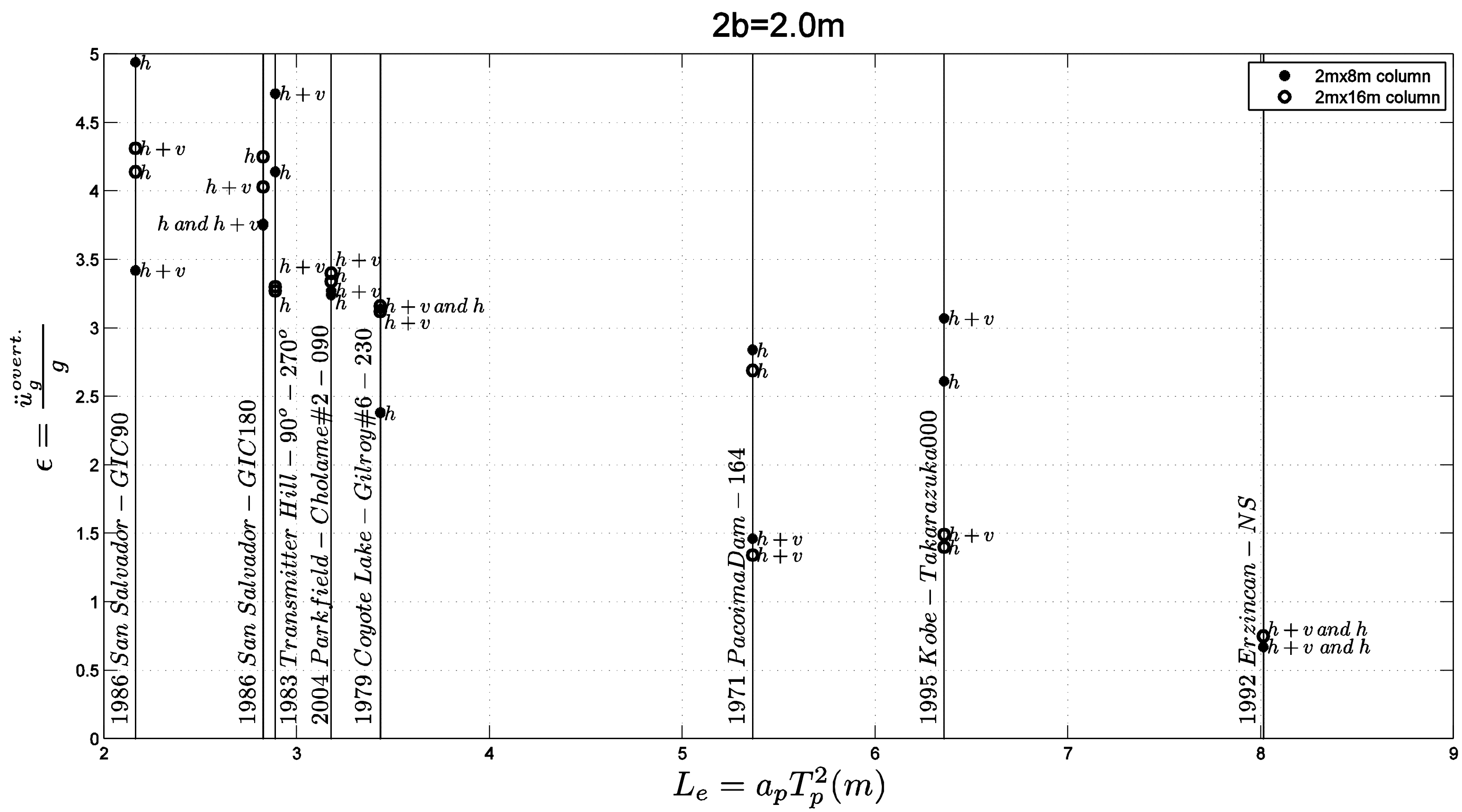

Figure 18. Overturning seismic coefficient, ε, of the amplified ground motions needed to overturn the monolithic column from the Temple of Apollo, Syracuse (dark dots) and a taller column with the same base $= 2.0m$ and twice the height (empty circles). The values of the overturning seismic coefficient, ε, are ordered with increasing length scale, $L_e = a_p T_p^{\ 2}$, of the dominant coherent acceleration pulse of the pulse-like record. The results exhibit a clear trend that is decreasing with the length scale, L_e.

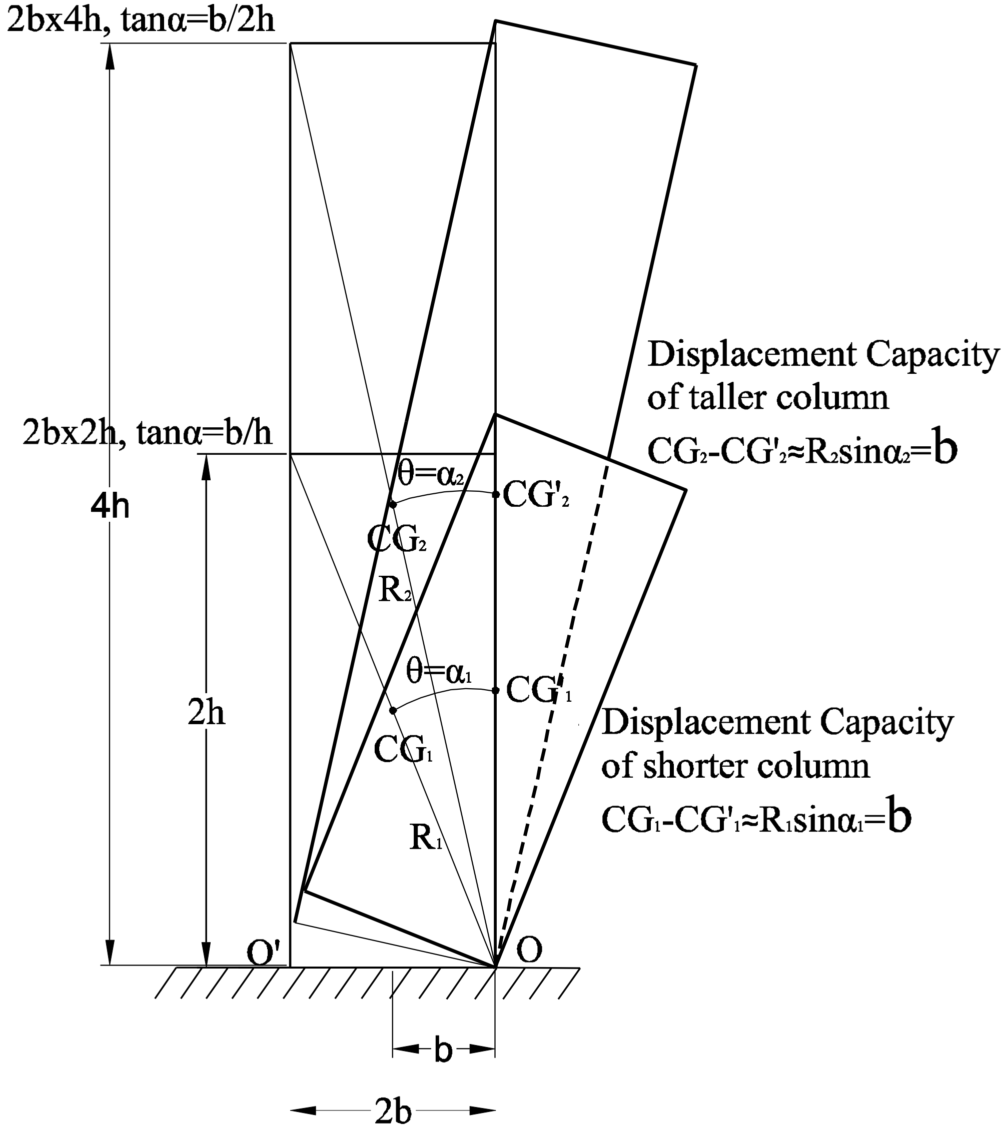

Figure 19. Two different height columns that have the same base $= 2b$, have the same seismic displacement capacity equal to half the base width, $b = R_i \sin \alpha_i$.

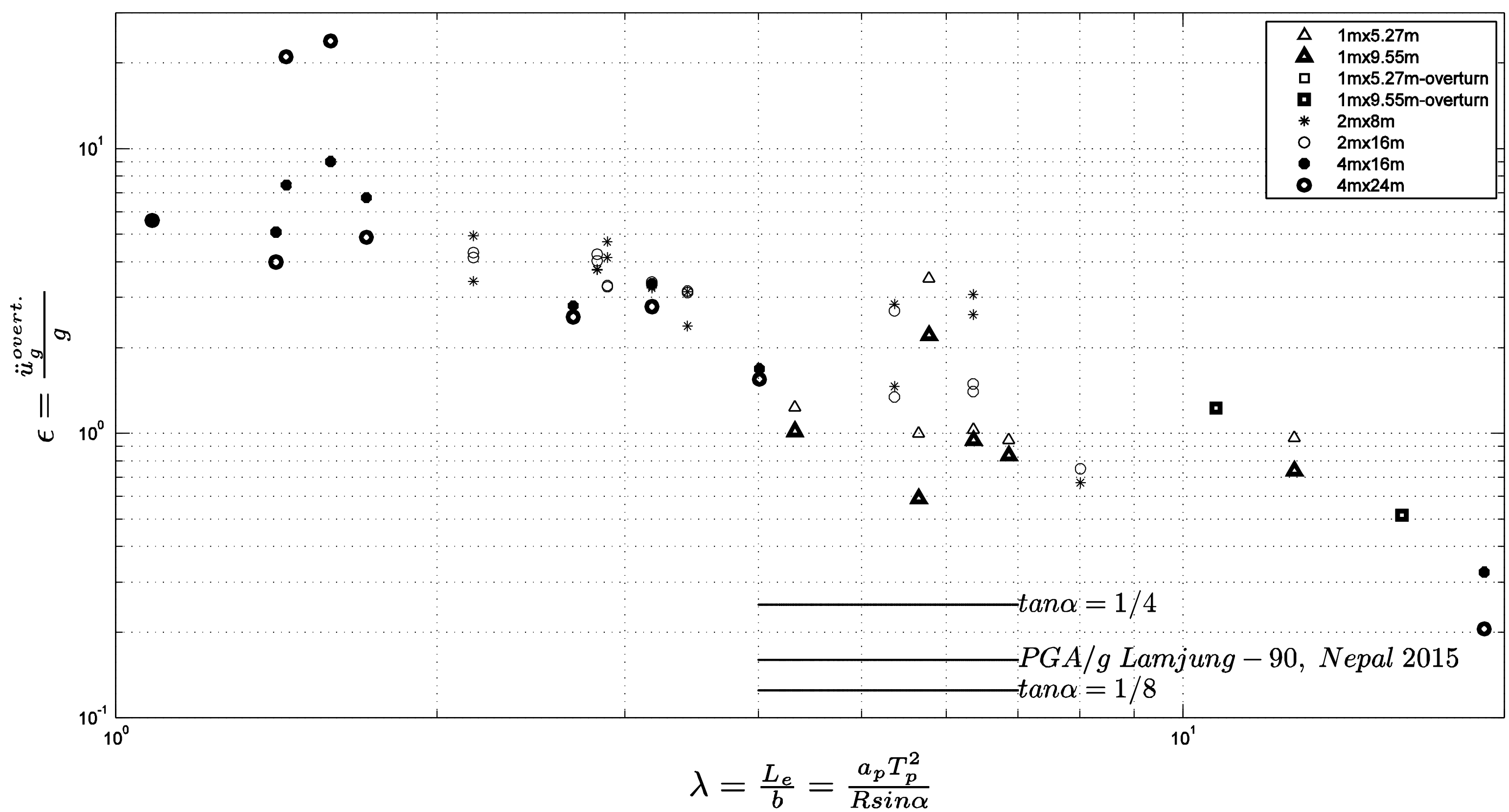

Figure 20. Overturning seismic coefficient, ε, of the amplified ground motions needed to overturn two columns with base $2b = 1.0m$ and height $2h = 5.27m$ and $9.55m$; two columns with base $2b = 2.0m$ and height $2h = 8.0m$ and $16.0m$; and two columns with base $2b = 4.0m$ and height $2h = 16.0m$ and $24.0m$. The values are plotted as a function of the proposed overturning potential index, λ, that is the ratio of the proposed overturning intensity measure, $L_e = a_p T_p^{\ 2}$, to the displacement capacity of the columns, $b = R\sin\alpha$. When $\lambda \geq 10$, any tall, free-standing column most likely overturns.

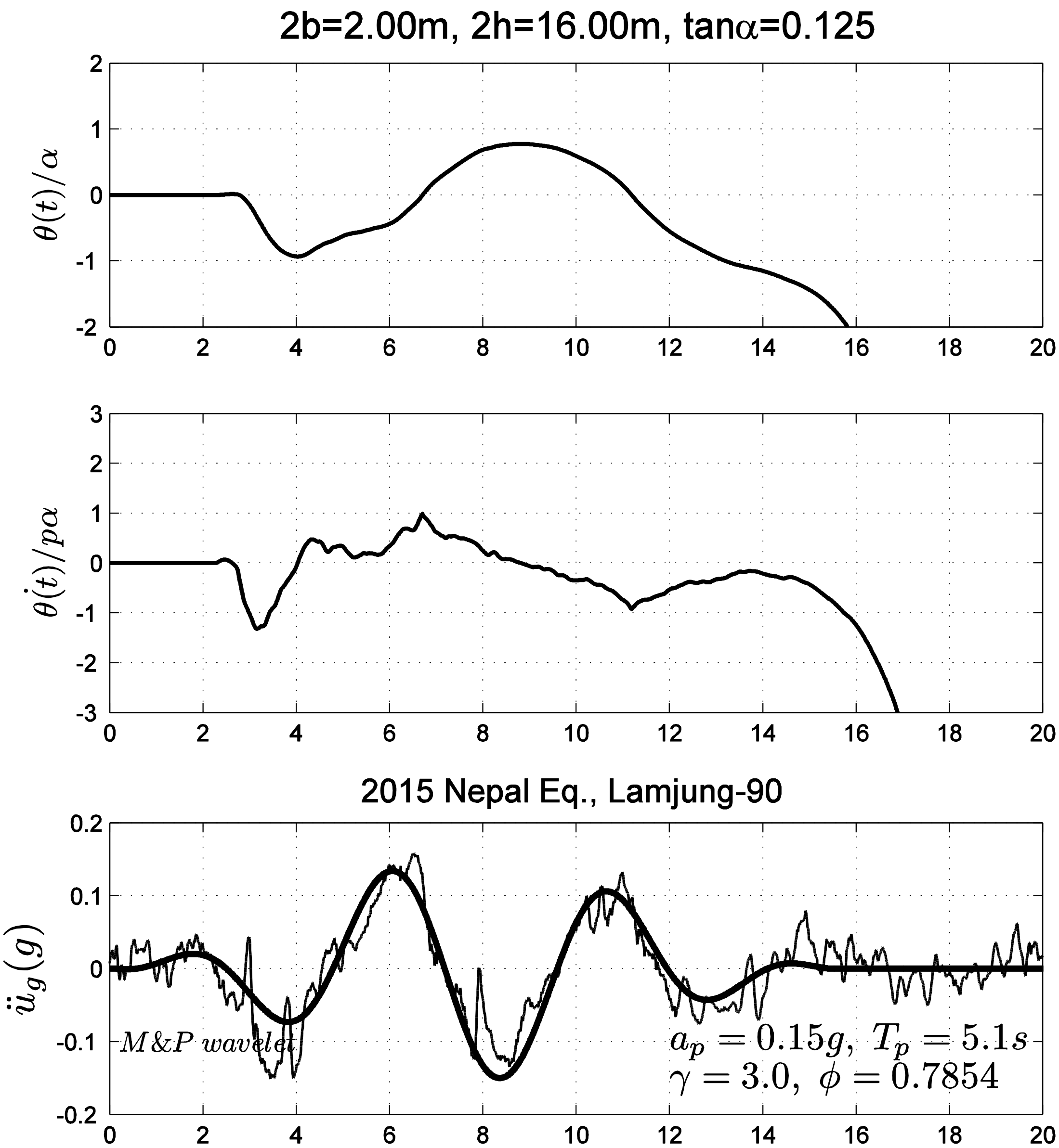

Figure 21. Rotation and angular velocity time histories of a $2.00m \times 16.00m$ column ($\tan\alpha = 0.125$) when excited by the horizontal component of the 2015 Nepal earthquake ($PGA = 0.158g$). The slightly larger $PGA = 0.158g$ than $g\tan\alpha = 0.125g$ is capable to induce overturning because of the very long duration ($T_p = 5.1s$) of the predominant pulse.